S100a9 lactylation triggers neutrophil trafficking and cardiac inflammation in myocardial ischemia/reperfusion injury

Xiaoqi Wang[1,2,#], Xiangyu Yan[1,2,#], Ge Mang[1,6,#], Yujia Chen[1,2], Shuang Liu[1,2], Jiayu Sui[1,2], Zhonghua Tong[1,2], Penghe Wang[1,2], Jingxuan Cui[1,2], Qiannan Yang[1,2], Yafei Zhang[1], Dongni Wang[1,2], Ping Sun[2,5], Weijun Song[1], Zexi Jin[1], Ming Shi[7], Peng Zhao[2,5], Jia Yang[1,2], Mingyang Liu[1], Naixin Wang[1,2], Tao Chen[1], Yong Ji[4,*], Bo Yu[1,2,3,*], Maomao Zhang[1,2,3,*]

[1]Department of Cardiology, the Second Affiliated Hospital of Harbin Medical University, Harbin, Heilongjiang Province, China. [2]The Key Laboratory of Myocardial Ischemia, Harbin Medical University, Ministry of Education, Harbin, Heilongjiang Province, China. [3]State Key Laboratory of Frigid Zone Cardiovascular Disease, Harbin, Heilongjiang, China. [4]Harbin Medical University, Harbin, China, [5]Department of Ultrasound (P.S.), the Second Affiliated Hospital of Harbin Medical University, Harbin, Heilongjiang Province, China. [6]Department of Cardiology, Beijing Anzhen Hospital, Capital Medical University, Beijing, China; [7]School of Life Science and Technology, Harbin Institute of Technology, Harbin, China. [#]These authors contributed equally. *These authors jointly supervised. **Addresses for Correspondence:**

*Maomao Zhang, Department of Cardiology, the Second Affiliated Hospital of Harbin Medical University, Harbin, China. Tel: +86-15145106466. Email: maomaolp1983@163.com.

*Bo Yu, Department of Cardiology, the Second Affiliated Hospital of Harbin Medical University, Harbin, China. Tel: +86-13804585601. Email: yubodr@163.com.

*Yong Ji, State Key Laboratory of Frigid Zone Cardiovascular Diseases, Harbin Medical University, Harbin, China. Tel: +86-0451-86615600. E-mail: yongji@hrbmu.edu.cn

Conflict of Interests: The authors have declared that no conflict of interest exists.

Graphical abstract

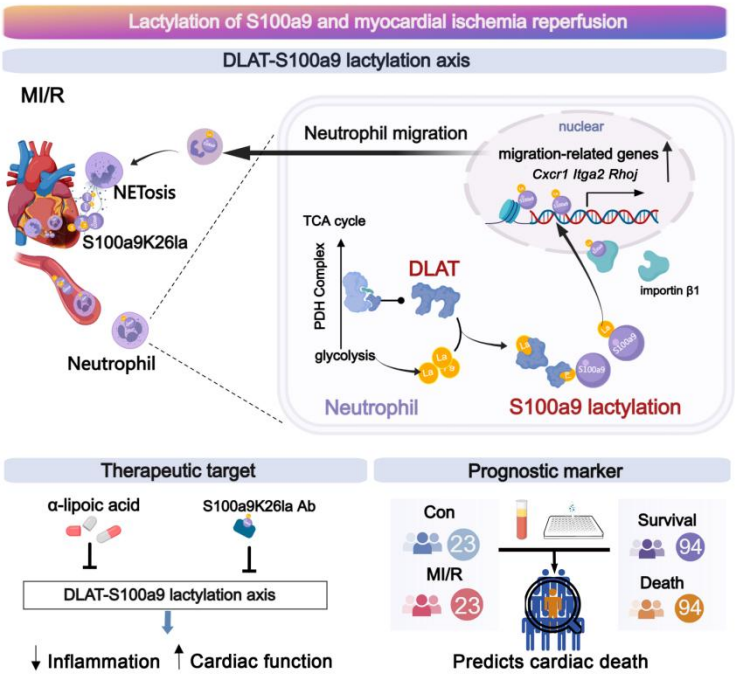

Abstract

Lactylation, a post-translational modification derived from glycolysis, plays a pivotal role in ischemic heart diseases. Neutrophils are predominantly glycolytic cells that trigger intensive inflammation of myocardial ischemia reperfusion (MI/R). However, whether lactylation regulates neutrophil function during MI/R remains unknown. Employing lactyl proteomics analysis, S100a9 was lactylated at lysine 26 (S100a9K26la) in neutrophils, with elevated levels observed in both acute myocardial infarction (AMI) patients and MI/R model mice. S100a9K26la was demonstrated driving the development of MI/R using mutant knock-in mice. Mechanistically, lactylated S100a9 translocated to the nucleus of neutrophils, where it binded to the promoters of migration-related genes, thereby enhancing their transcription as a co-activator and promoting neutrophil migration and cardiac recruitment. Additionally, lactylated S100a9 was released during NETosis, leading to cardiomyocyte death by disrupting mitochondrial function. The enzyme dihydrolipoyllysine-residue acetyltransferase (DLAT) was identified as the lactyltransferase facilitating neutrophil S100a9K26la post-MI/R, a process that could be restrained by α-lipoic acid. Consistently, targeting DLAT/S100a9K26la axis suppressed neutrophil burden and improved cardiac function post-MI/R. In patients with AMI, elevated S100a9K26la levels in plasma were positively correlated with cardiac death. These findings highlight S100a9 lactylation as a potential therapeutic target for MI/R and as a promising biomarker for evaluating poor prognosis of MI/R.

Keywords: Neutrophil, Lactylation, S100a9, Migration, Myocardial ischemia-reperfusion

Introduction

Reperfusion therapies can effectively restore blood flow to the ischemic myocardium in time, yet mortality rates remain high because of additional heart damage caused by reperfusion injury (1, 2). As sentinels of inflammation, neutrophils are mobilized and recruited to the infarcted heart. High neutrophil count is a causal risk factor for ischemic heart disease (3). Prompt mitigation of the neutrophil burden may prevent adverse remodeling and improve cardiac outcomes (4). However, effective pharmacological treatments targeting acute neutrophil recruitment are still unavailable.

The significance of epigenetic modifiers and their genetic manipulation in influencing neutrophil behavior has been increasingly recognized (5-7). Neutrophil metabolism primarily relies on glycolysis under steady-state conditions and undergoes reprogramming to increase glycolysis during acute inflammatory attacks as previously reported (8, 9). This metabolic shift produces lactate (10), which serves as a precursor to stimulate lactylation (11).

Protein lactylation, as a form of epigenetic modification (11), appears to have some substantial effects in regulating cellular functions in various cardiovascular diseases, including atherosclerosis, heart failure, cardiac fibrosis, and myocardial infarction (MI) (12-15). Our previous study suggested that histone lactylation directly boosts the reparative transcriptional response in monocytes post-MI (13). However, there is a lack of studies investigating the distribution and role of overall protein lactylation in neutrophils post-myocardial ischemia reperfusion (MI/R). Through proteomics analysis, we identified an alarmin protein S100a9 lysine 26 (S100a9K26) as the primary modification target of early, remotely elevated neutrophil lactylation post-MI/R. S100a8/a9 plays a critical role in inducing robust inflammation upon release (16). However, the function of lactylated S100a9 in neutrophils post-MI/R remains unclear.

In this study, we provided, to our knowledge, the first evidence that the elevation of

S100a9 lactylation aggravates cardiac dysfunction post-MI/R. We identified dihydrolipoyllysine-residue acetyltransferase (DLAT), a component of pyruvate dehydrogenase (PDH) complex (17), was a lactyltransferase directly catalyzing lactylation of S100a9. Our findings highlight lactylation-related signaling as a potential therapeutic target for MI/R.

Results

S100a9 lactylation is elevated in neutrophils after myocardial ischemia-reperfusion

Among several post-translational modifications including crotonylation, phosphorylation, acetylation, and lactylation, only pan-lactylation exhibited a significantly upregulation in the neutrophils on day 1 post-MI/R (Supplementary Figure 1A). Since lactylation is derived from glycolytic stress, we directed our attention at neutrophil lactylation post-MI/R. Pan-lactylation globally increased in the peripheral blood and cardiac-infiltrating neutrophils on day 1 post-MI/R (Supplementary Figure 1, B and C).

To evaluate the significance of neutrophil lactylation in MI/R, we conducted proteomics and lactylation modification proteomics of bone marrow (BM) neutrophils from sham and MI/R mice on day 1. Motif analysis revealed an overrepresentation of glycine (G), whereas glutamine (Q) and arginine (R) were less abundant than expected at the −1 and +1 positions surrounding the lactylation sites (Supplementary Figure S1D). Kla proteins were predominantly concentrated in the nucleus followed by the cytoplasm (Supplementary Figure S1E). On day 1 post-MI/R, 505 proteins exhibited a substantial increase in expression, indicating substantial association with leukocyte migration and chemotaxis (Figure 1A and Supplementary Figure 1F). Compared to the sham group, 71 proteins exhibited a substantial upregulation of Kla at 92 sites, while 27 proteins showed notable downregulation of Kla at 29 sites, with 73.9% of the sites displaying exclusive Kla alterations (Figure 1B). The top 10

Gene Ontology (GO) terms associated with Kla-modified proteins were mainly enriched in myeloid leukocyte migration, innate immune response (Figure 1C). Additionally, Kla-modified proteins were prominently represented by the S100/calbindin-D9K domains, including S100a8, S100a9, and S100a11 (Figure 1D). Among these proteins, lysine at position 26 of S100a9 (S100a9K26) exhibited the highest modification intensity by lactylation post-MI/R, as indicated by the ranking of their relative lactylation ratios (Figure 1E). Intriguingly, the K26 residue is located in the conserved calgranulin domain of S100a9 (Figure 1F and Supplementary 1G). Thus, we identified S100a9K26 as a potential target of neutrophil lactylation post-MI/R and presented its representative mass spectrum (MS, Figure 1G). We generated an S100a9K26la-specific antibody through K26 lactylated peptides (Supplementary Figure 2B). To verify its specificity, we performed dot blot assays using lactylated peptides and unlactylated peptides and co-immunoprecipitation (CoIP) analysis of 32Dcl3-induced neutrophils with K26 arginine (R) and glutamine (Q) mutants, which mimicked the delactylated state of the protein (Supplementary Figure 2, A–D). As expected, both the K26R and K26Q mutants exhibited lower S100a9K26la levels. Intriguingly, the pan-lactylation of S100a9 in immunoprecipitated K26R or K26Q mutants was also lower than that in the wild-type (WT) counterpart (Supplementary Figure 2E), indicating that K26 was the primary lactylation site of S100a9. Moreover, the K26R and K26Q mutants did not alter the levels of S100a8 in the flag-S100a9 complex, indicating that the mutation at the K26 locus and lactylation did not affect the binding of S100a8 with S100a9 (Supplementary Figure 2E).

Subsequently, we identified the expression profile of S100a9K26la in immune cells in heart, blood and BM 1 d post-MI/R. S100a9K26la was mostly originated from neutrophils rather than monocytes/macrophages or dendritic cells in heart, blood and BM 1 d post-MI/R (Supplementary Figure 3, A–D). Compared to the sham surgery group, S100a9K26la was highly increased in neutrophils of heart, blood and BM 1 d after reperfusion (Supplementary Figure 3, E–G). Therefore, we assessed dynamic changes in S100a9K26la levels in

neutrophils post-MI/R. Immunoblots of BM and circulating neutrophils at various time points post-MI/R revealed a significant upregulation of S100a9K26la (normalized to β-actin) at 24 h, which returned to the baseline levels by 72 h post-MI/R (Figure 1, H–K). Compared to S100a9, S100a9K26la (normalized to S100a9) in both BM and blood neutrophils notably increased at 12 h post-MI/R (Supplementary Figure 1, H and I). Consistently, we found sustained cardiac neutrophil S100a9 lactylation throughout the early stages of MI/R, but no significant change in S100a9 lactylation of cardiomyocytes (Figure 1L and Supplementary Figure 1K).

To validate this discovery in human, we examined S100a9K26la levels in circulating neutrophils and plasma between patients with acute myocardial infarction (AMI) receiving percutaneous coronary intervention (PCI) within 24 h and those with unstable angina (UA) (Figure 1M and Supplementary Table 1). Both intracellular S100a9K26la levels in circulating neutrophils and plasma S100a9K26la showed a notable increase in patients with AMI after PCI (Figure 1, N and O, Supplementary Figure 1, K and L). Moreover, plasma S100a9K26la levels were significantly correlated with cardiac troponin I (cTnI) levels (Figure 1P).

In brief, neutrophil S100a9K26 lactylation elevated early and extensively post-MI/R.

K26 mutation of S100a9 alleviates deleterious inflammation and cardiac dysfunction post-MI/R

To explore the role of S100a9K26la in MI/R, we constructed S100a9K26R mutant mice to abolish S100a9K26 lactylation, achieved by mutating lysine 26 (AAG) to arginine (CGT) (Figure 2, A and B). S100a9K26R mice exhibited lower plasma levels of inflammatory cytokines on day 1 post-MI/R (Supplementary Figure 5, A–C). According to the histopathological analysis, the hearts of S100a9K26R mice exhibited reduced inflammatory cell infiltration compared to those of WT mice on day 3 post-MI/R (Figure 2C). Immunofluorescence analysis revealed diminished neutrophils and myeloperoxidase (MPO)

levels in S100a9K26R heart on day 1 post-MI/R (Supplementary Figure 5D). Further flow cytometry analysis revealed that at 1 and 3 days post-MI/R, neutrophils, ly6C^{hi} monocytes and dendritic cells were notably inhibited in S100a9K26R hearts compared with WT hearts (Supplementary Figure 4, A–E). However, both CD4$^+$ and CD8$^+$ T cells did not differ between WT and S100a9K26R hearts (Supplementary Figure 4, F–H). Subsequently, S100a9K26R reduced the expression levels of collagen genes and fibrosis-related genes in the heart on day 3 and 7 post-MI/R (Supplementary Figure 5G), as well as improved cardiac fibrosis at day 14 post-MI/R (Figure 2, D and E). Additionally, S100a9K26R mice showed a non-significant trend toward improved survival and reduced cardiac rupture incidence compared to WT controls (Supplementary Figure 5, E and F). Importantly, S100a9K26R mice showed significant improvements in post-injury ejection fraction (EF) and fractional shortening (FS), accompanied by a notable decrease in ventricular internal diameter end systole (LVIDs, Figure 2, F and G). These findings indicate that the global deletion of S100a9K26la ameliorates MI/R.

We further constructed the myeloid cell S100a9K26la deletion mice by bone marrow transplantation (BMT). In brief, the BM from WT and S100a9K26R mice was transplanted into WT mice before MI/R surgery (Figure 2H). The rate of engraftment was shown in Supplementary Figure 5K. As expected, the myeloid cell-specific S100a9K26R mutant dramatically suppressed inflammation and cardiac fibrosis and dysfunction post-MI/R (Figure 2, I–M, Supplementary Figure 5, H–J). Additionally, we performed rescue experiments using recombinant non-lactylated S100a9 following myeloid-specific deletion of S100a9K26la post-MI/R (Figure 2H). The treatment of recombinant S100a9 (rS100a9) remarkably induced inflammation and cardiac dysfunction in MI/R mice with WT donors. However, compared with the MI/R mice with WT donors, the MI/R mice with S100a9K26R donors significantly reduced the inflammation and cardiac dysfunction induced by rS100a9, highlighting the specific damage to MI/R mice of S100a9K26la that differs from those of S100a9 (Figure 2, I–

M, Supplementary Figure 5, H–J).

To confirm the specific role of S100a9K26la in neutrophils to MI/R, we injected recipients intravenously 1 hour post-MI/R with $Ly6G^+$ neutrophils from either the BM of WT or S100a9K26R mice (Supplementary Figure 6, A and B). The efficiency of adoptive transfer (AT) was shown in Supplementary Figure 6C. As expected, the mice receiving S100a9K26R neutrophils displayed significantly reduction of immune cell infiltration and improvement of cardiac dysfunction (Supplementary Figure 6, D–J). Nevertheless, the transfer of S100a9K26R myeloid cells excluding neutrophils did not result in any improvement in inflammation and cardiac dysfunction (Supplementary Figure 6, K–T). These findings suggest that targeting lysine at the S100a9K26 site to suppress S100a9K26la of neutrophils yields favorable outcomes post-MI/R.

Lactylated S100a9 is released via NETs and triggers cardiomyocyte death by impairing mitochondrial function

As S100a9 is widely recognized as a secreted alarmin, we checked the lactylated S100a9 in plasma post MI/R through indirect ELISA. In mice model, similar to unlactylated S100a9, lactylated S100a9 increased until 72 h post-MI/R compared with the sham-operated mice (Figure 3A and Supplementary Figure 7A). Given that a proportion of S100a9 is bound to neutrophil extracellular traps (NETs) (18), we hypothesized that lactylated S100a9 is released by NETosis. We found a robust increase in a specific marker histone H3 citrulline (H3Cit) of NETs, as well as colocalization of S100a9K26la with H3Cit in the cardiac infiltrated neutrophils after MI/R as well as the isolated neutrophils after phorbol myristate acetate (PMA) treatment for 4h (Figure 3, B and D). Flow cytometry analysis also confirmed the $S100a9K26la^+$ $H3Cit^+$ neutrophils (Supplementary Figure 7E). We established a *Padi4* knockout mice, an enzyme that is critical for citrullination of histones and NETs, followed by MI/R injury. Deficiency of *Padi4* resulted in a significantly decrease in plasma S100a9K26la

levels, S100a9 levels as well as H3cit levels day 1 post-MI/R (Figure 3C and Supplementary Figure 7, B and C). To link NETs directly with S100a9K26la extracellular release in neutrophils, we treated BM neutrophils from *Padi4*$^{-/-}$ or WT mice with PMA for 4h. We observed a robust increase of S100a9K29la levels in PMA-treated WT neutrophil supernatant compared to the vehicle group and a notable reduction of S100a9K29la levels in *Padi4*$^{-/-}$ cell supernatant compared to the WT, which was consistent with S100a9 (Figure 3E and Supplementary Figure 7D). These results suggest that NETs is required for the secreted S100a9K26la.

Extracellular S100a8/a9 was reported to trigger cardiomyocyte death by impairing mitochondrion (18). In vitro, BM neutrophils were treated with or without PMA for 4h, then collected the conditioned medium or NETs to co-culture with mouse neonatal cardiomyocytes (NCMs). The NETs but not the conditional medium contributed to cardiomyocyte death by impairing mitochondrion (Supplementary Figure 8, A–F). To explore whether lactylated S100a9 directly caused CM death like S100a9, NCMs were co-cultured with NETs from WT, S100a9K26R and *S100a9*$^{-/-}$ neutrophils stimulated by PMA. Compared with vehicle, the NETs from PMA-treated WT neutrophils notably inhibited ATP production, and increased the mitochondrial membrane potential loss in NCMs, resulting in increased NCM death (Figure 3, F–J). Compared with the NETs from WT neutrophils, the NETs from S100a9K26R neutrophils exposed to PMA induced ATP production, declined the mitochondrial membrane potential loss in NCMs, and attenuated NCM death (Figure 3, F–J). However, DNase I (inhibitor of NETs) eliminated the difference between the WT and S100a9K26R neutrophils (Supplementary Figure 7, G–K). In addition, the NETs from *Padi4*$^{-/-}$ neutrophils also reduced mitochondrial dysfunction and NCM death compared to the NETs from WT neutrophils (Supplementary Figure 8, G–K). To note, S100a9K26R and *S100a9*$^{-/-}$ neutrophils displayed no difference in improving mitochondrial dysfunction and NCM death caused by PMA-treated WT neutrophils (Supplementary Figure 7, G–K). Furthermore, BM neutrophils were

isolated from WT, S100a9K26R and *S100a9*$^{-/-}$ mice on sham-operated or day 1 MI/R, then NETs were collected to co-culture with NCMs in the presence or absence of DNase I. This ex vivo experiment also confirmed that lactylated S100a9 was released via NETosis and directly impaired mitochondrion and caused CM death, but lactylation did not contribute to additional cardiomyocyte death caused by unlactylated S100a9 (Supplementary Figure 7F and Supplementary Figure 8, L–P).

Lactylated S100a9 translocated into the nucleus and boosts the transcription of intracellular signals directing neutrophil migration

To explore the role of lactylated S100a9 within intracellular of neutrophils, we examined the distribution of S100a9K26la and found the strong nuclear localization of S100a9K26la in neutrophils post-MI/R (Figure 4A). Confocal analysis of circulating neutrophils on day 1 post-MI/R confirmed a strong increase in nuclear S100a9K26la following MI/R (Supplementary Figure 9A). Employing CoIP coupling MS, we found that S100a9K26la was bound to importin β1, which was further confirmed using CoIP analysis (Supplementary Figure 9, B–D). The importin β1 inhibitor blocked the translocation of S100a9K26la into nuclei, leading to a decrease in nuclear S100a9K26la (Supplementary Figure 9E). Additionally, in circulating neutrophils, S100a9K26la was observed to bind to histones, and its fractions were identified within nuclear proteins using MS (Supplementary Figure 9, F and G). These findings suggest that S100a9K26la translocates into nuclei in an importin β1-dependent manner and potentially regulates or influences gene transcription.

Next, we performed Cleavage Under Targets and Tagmentation (CUT-Tag) assays of circulating neutrophils from sham-operated and MI/R-mice 24 h post-MI/R using anti-S100a9K26la and anti-S100a9 antibodies (Supplementary Figure 10A). S100a9K26la was predominantly enriched in the promoter regions of these genes (Supplementary Figure 10B). The majority of genes exhibiting increased S100a9K26la marking were not marked by

S100a9. S100a9K26la marked more genes (61% of all genes marked by S100a9K26la or S100a9) than those marked by S100a9 (39% of all marked genes). (Figure 4B). S100a9K26la-specific genes had a substantial impact on genes involved in cell migration and adhesion, while the S100a9-specific genes were enriched in the positive regulation of the force of heart contraction (Figure 4C and Supplementary Figure 10C). To identify S100a9K26la-target genes in neutrophils post-MI/R, we integrated the CUT-Tag and RNA-seq data of circulating neutrophils from sham and MI/R-mice 24 h post-MI/R and then classified the genes into four categories based on their expression levels and S100a9K26la modification (Figure 4D). Genes with altered expressions that were marked by S100a9K26la underwent various biological processes. As expected, upregulated genes with S100a9K26la binding were largely associated with cell migration and adhesion (Figure 4E). Key intracellular signals for cell migration included chemokine receptors, Rho and Rac GTPase signals governing neutrophil polarization, and adhesion receptor integrins (Figure 4F). Based on the fold-change rank of the S100a9K26la binding signal, integrin alpha 2 (*Itga2)*, ras homolog family member J (*Rhoj)*, and C-X-C motif chemokine receptor 1 (*Cxcr1)* were substantially upregulated (Figure 4F).

We further conducted RT-qPCR and chromatin immunoprecipitation-qPCR (ChIP-qPCR) analysis to confirm the increased expression and S100a9K26la enrichment in the promoter regions of Itga*2*, *Rhoj*, and *Cxcr1* in circulating neutrophils 24 h post-MI/R. Deletion of S100a9K26la sharply attenuated the messenger RNA (mRNA) levels and the S100a9K26la marks at the *Itga2*, *Rhoj*, and *Cxcr1* promoters (Figure 4, G–H). Furthermore, a genomic snapshot suggested that S100a9K26la strongly binds to *Itga2*, *Rhoj*, and *Cxcr1*, whereas the binding of S100a9 was weak (Supplementary Figure 10D). ChIP-qPCR analysis of S100a9 indicated that S100a9 did not enrich in the target genes and did not contribute to migratory gene activity (Supplementary Figure 10E).

We further established BM neutrophils-activated models in vitro with lipopolysaccharide (LPS) stimulation for 4h, and the glycolysis and S100a9 lactylation in activated neutrophils dramatically increased (Supplementary Figure 11, A–C). Then activated-BM neutrophils were treated with exogenous sodium lactate (NaLa) or the lactate dehydrogenase inhibitor sodium oxamate (Oxa) for 4 h. Exogenous NaLa promoted S100a9K26la levels in a dose-dependent manner, leading to the increased mRNA expression of *Itga2*, *Rhoj*, and *Cxcr1*, along with increased S100a9K26la marks at their promoter regions and enhanced neutrophil migratory ability, whereas Oxa attenuated these effects (Supplementary Figure 11, D–K). Therefore, *Itga2*, *Rhoj*, and *Cxcr1* were identified as potential targets of neutrophil S100a9K26la following MI/R.

Collectively, S100a9K26la acts as a co-activator and selectively binds to the promoter region of target genes, thereby directly promoting the expression of migration-related molecules post-MI/R.

S100a9K26R suppresses neutrophil migration and recruitment post-MI/R

RNA-seq analysis on neutrophils isolated from blood and heart of the S100a9K26R and WT on day 1 post-MI/R revealed the inhibition of migration-related pathways in S100a9K26R neutrophils from blood and heart (Supplementary Figure 12, A and B). The expression of genes involved in neutrophil migration, such as integrins and chemokine receptors, was significantly reduced in the blood and heart of S100a9K26R mice owing to the lack of S100a9K26la (Supplementary Figure 12C). Therefore, S100a9K26R damages the migratory transcriptional landscape of neutrophils. Notably, S100a9K26R mice exhibited decreased protein expression of CXCR1, CXCR2 (C-X-C chemokine receptor 2), Mac-1 (integrin αMβ2), and, LFA-1 (lymphocyte function-associated antigen-1) of neutrophils from the blood and BM on day 1 post-MI/R compared to WT (Supplementary Figure 12, D–G). Consistently, the Transwell assay and neutrophil polarization analysis confirmed that

S100a9K26R neutrophils isolated from the BM on day 1 post-MI/R exhibited significantly impaired migration toward CXCL2 (C-X-C motif chemokine ligand 2) in vitro (Figure 4, J and K). In static adhesion on endothelial cells in vitro, in the presence of Mg^{2+}, there was significantly reduced adhesion of S100a9K26R neutrophils on TNF-α–treated mouse cardiac microvascular endothelial cells (CMEC) compared with WT controls (Figure 4I), indicating an adhesion defect of S100a9K26R neutrophils. Additionally, S100a9K26R neutrophils also exhibited significantly impaired adhesion and polarization on the integrin ligand–ICAM-1 (intercellular cell adhesion molecule-1, Supplementary Figure 12, H–J). Importantly, addition of functional blocking antibodies specific for Mac-1 or LFA-1 markedly reduced the adhesion and polarization of WT neutrophils on ICAM-1, without further inhibiting the defective adhesion and polarization of S100a9K26R neutrophils (Supplementary Figure 12, H–J). During the acute setting of MI/R, S100a9K26R significantly reduced neutrophil accumulation in both the blood and injured heart, but increased the retention of neutrophils in BM (Figure 4, L and M, Supplementary Figure 12K). Furthermore, we observed no difference in the frequency of apoptotic neutrophils in the heart, blood, and BM between WT and S100a9K26R mice day 1 post-MI/R (Supplementary Figure 12, L–N), suggesting that neutrophil apoptosis is not the cause of reduced cardiac neutrophil counts in S100a9K26R MI/R mice. Thus, S100a9K26R leads to defective neutrophil migration and the reduction of cardiac neutrophil accumulation post-MI/R due to deletion of S100a9K26-specific lactylation.

DLAT directly catalyzes S100a9 lactylation in neutrophils

To determine the underlying enzyme that catalyzed S100a9 lactylation in neutrophils, we analysed anti-S100a9K26la immunoprecipitates from BM neutrophils day 1 post-MI/R by MS. As shown in Figure 5A, DLAT was the protein that most substantially binds to S100a9K26la. DLAT functions to catalyze protein acetylation as reported (17, 19), thus we asked whether it lactylated S100a9 (Figure 5B). The interaction between DLAT and

S100a9K26la was validated by reciprocal IP analyses with either an anti-S100a9K26la or an anti-DLAT antibody (Figure 5C), and was primarily localized in the cytosol (Supplementary Figure 13A).

We further used purified recombinant protein of DLAT to examine its interaction with lactyl-CoA by surface plasmon resonance (SPR) assay. Indeed, lactyl-CoA was found to bind DLAT with a Kd value of 65.3 μM, as did the positive control acetyl-CoA (Kd = 240 μM) (Figure 5D). In vitro lactylation experiments suggested that DLAT lactylated S100a9 (Figure 5E). Moreover, knockdown of DLAT in neutrophils by small interfering RNA (siRNA) remarkably inhibited the lactylation levels of S100a9 (Figure 5F and Supplementary Figure 13B). Furthermore, molecular docking analysis indicated that amino acid residues of DLAT interacted with lactyl-CoA through hydrogen bond (Figure 5G), and the critical residues with the top average energy values was isoleucine 423 (I423), as dynamics simulations indicated (Figure 5H). Therefore, we generated catalytically fewer active forms of DLAT (I423A, Alanine), which demonstrated decreased ability to lactylate S100a9 at K26 compared to the corresponding control WT acetyltransferases in the in vitro lactyltransferase activity assay (Figure 5I and Supplementary Figure 13C). Therefore, DLAT is the potential lactyltransferase of S100a9 lactylation, which catalytical activity depends on critical residues I423.

Lipoic acid is a typical substrate of DLAT, promoting DLAT lipoacylation and PDH activity, leading to increased acetyl-CoA (20, 21). Consistently, the treatment of α-lipoic acid (ALA) significantly increased the DLAT lipoacylation and PDH activity, as well as the acetyl-CoA level in neutrophils, while the deletion of S100a9K26la did not affect the PDH activity and acetyl-CoA level (Figure 5, J and K, Supplementary Figure 13, D–F). Instead, ALA inhibited S100a9 lactylation and the binding of S100a9K26la to DLAT (Figure 5J and Supplementary Figure 13D). This might be due to the competitive combination of ALA or the acetyl-CoA to DLAT. To test this hypothesis, we generated de-lipoacylated DLAT by

mutating both K131 and K258 residues to R, which showed increased ability to catalyze S100a9 lactylation compared to the corresponding WT (Figure 5L and Supplementary Figure 13G). Moreover, the presence of acetyl-CoA reduced the S100a9 lactylation level (Figure 5M and Supplementary Figure 13H), suggesting ALA served as a lactyltransferase inhibitor due to providing a lipoacyl group and inducing acetyl-CoA. Actually, according to the SPR assay, lactyl-CoA revealed higher efficient binding affinity to DLAT than acetyl-CoA or ALA (Figure 5, N and O), which was further verified by a cellular thermal shift assay (CETSA, Figure 5, P and Q). Therefore, DLAT-mediated S100a9 lactylation in neutrophils can be efficiently antagonized by ALA.

Targeting DLAT/S100a9K26la signaling improves acute inflammation and cardiac dysfunction post MI/R.

Given that ALA is a S100a9 lactylation inhibitor, we next determined whether ALA could mitigate MI/R injury. WT mice were intraperitoneally injected with the ALA or vehicle before and after MI/R (Figure 6A). In ALA-treated mice, S100a9K26la level in circulating neutrophils significantly decreased, which resulted in a significant reduction of S100a9K26la marks on target genes and the mRNA expression of these genes (Figure 6, B–D), as well as the expression levels of adhesion molecules of neutrophils (Supplementary Figure 14, L and M) Consistently, the neutrophils from BM treated with ALA displayed a damaged ability to migrate toward CXCL2 compared to the vehicle (Figure 6E). Moreover, ALA injection significantly inhibited neutrophils and Ly6C^{hi} monocytes and macrophages infiltration in heart post-MI/R (Figure 6, F and G). Gating strategy for identification of leukocytes was shown in Supplementary Figure 16, A and B. Consistently, CM death, determined by TUNEL and cTnI double staining, was markedly reduced in ALA-treated mice compared to WT mice after MI/R (Figures 6H). Importantly, ALA-treated mice showed significant improvements in post-injury EF and FS 14 days post-MI/R (Figure 6, I–K). Furthermore, we observed that

administration of ALA markedly mitigated MI/R in a dose dependent manner through inhibiting S100a9K26la levels, reducing neutrophil cardiac recruitment and CM death, and improving cardiac dysfunction (Supplementary Figure 14, A–K).

Additionally, S100a9K26la custom antibodies were adopted to block S100a9K26la. To test whether S100a9K26la neutralizing antibodies could enter the cells, we isolated circulating neutrophils from WT mice 1 day post-MI/R and treated them with 10 ug S100a9K26la antibody or IgG conjugated with 488 dye for 2 h. Immunofluorescence showed that S100a9K26la antibody conjugated with 488 dye (green) was located in the intracellular of neutrophils (Supplementary Figure 15A). Using Horseradish Peroxidase (HRP)-coupled anti-rabbit-IgG antibodies directly incubating polyvinylidene fluoride (PVDF) membrane containing neutrophil cytoplasmic protein, we visualized cytosolic S100a9K26la antibody (Supplementary Figure 15B). These data suggested that antibody could enter the cells. Furthermore, functional analysis using ChIP-PCR, PCR, and Transwell suggested that, compared with IgG, S100a9K26la antibody inhibited the S100a9K26la marks on target genes and the mRNA expression of these genes in neutrophils, as well as the neutrophil migratory ability (Supplementary Figure 15, C–E). In summary, S100a9K26la antibody entered the neutrophils partially via caveolae-dependent endocytosis and inhibited the transcription of target genes and neutrophil migratory ability. In vivo, S100a9K26la custom antibodies reduced inflammatory cytokines levels in plasma, inhibited the neutrophils and Ly6C^{hi} monocytes and macrophages accumulation in blood and heart, and improved myocardial fibrosis and cardiac dysfunction post-MI/R (Supplementary Figure 15, F–L).

S100a9K26la is associated with cardiac death in AMI patients undergoing PCI

To further evaluate the clinical utility of S100a9K26la in predicting cardiac risk following MI/R injury, we conducted a retrospective study involving 188 patients with AMI who presented within 12 h of symptom onset and underwent PCI within 24 h. Among these

patients, 94 were categorized as high-risk AMI patients who experienced cardiac death within a 1-year follow-up period, while the remaining 94 low-risk patients survived (Figure 7A, Supplementary Table 2). Both S100a9K26la and S100a9 levels were significantly elevated in AMI patients with cardiac death compared to survivors post-PCI (Figure 7B and Supplementary Figure 17B). Additionally, S100a9K26la exhibited significant associations with baseline myocardial injury markers (creatine kinase isoenzyme MB, CK-MB and cardiac troponin I, cTnI) and baseline cardiac function indexes (left ventricular ejection fraction, LVEF and N-terminal pro-brain natriuretic peptide, NT-proBNP), while S100a9 showed no such associations with myocardial injury markers (Figure 7C and Supplementary Table 3). To note, during the follow-up period, the frequency of intercurrent heart failure (HF) events was significantly increased in the death cases compared to the survivor-matched controls. However, there was no difference in the frequency of recurrent MI between these two groups (Supplementary Figure 17G). Additionally, S100a9K26la levels were remarkably negatively correlated with LVEF at the first month follow-up in AMI patients (Supplementary Figure 17H). We also observed a consistent negative trend but statistically non-significant association between S100a9K26la levels and LVEF at the 3rd, 6th, and 12th month follow-up in AMI patients (Supplementary Figure 17I). We further analyzed 55 pairs of patients who survived or experienced cardiac death during the follow-up period by conducting an RNA-seq analysis to delineate transcriptional profiles associated with high-risk AMI patients with cardiac death. The differential expressed genes between survivors and deceased patients were substantially enriched in pathways related to inflammatory responses and neutrophil chemotaxis (Figure 7D and Supplementary Figure 17A). Subsequent gene set enrichment analysis (GSEA) indicated that the predominant pathological process underlying cardiac death was associated with neutrophil migration and neutrophil chemotaxis (Figure 7E). S100a9K26la levels exhibited a significant correlation with interleukin-1 beta (IL-1β) expression (Figure 7F). The hazard ratio (HR) analysis revealed that elevated S100a9K26la

levels were associated with a significantly increased risk of cardiac death (HR 2.168 (1.389, 3.384), Figure 7G). Importantly, based on the optimal cut-off value, patients with high S100a9K26la levels (≥37.125 × 10^5pg/mL) on day 1 post-PCI were more likely to experience cardiac death during long-term follow-up (Figure 7G). Furthermore, considering that bacterial stimulation can induce lactate production and lactylation, we excluded the patients with infection (Supplementary Table 4). S100a9K26la also served as a marker associated with a heightened risk of cardiac death and relatively poor outcomes in AMI patients without infections (Supplementary Figure 17, C–F).

Discussion

The early burst of excessive inflammation after AMI contributes to reperfusion injury (1). Despite the benefits of anti-inflammatory therapies targeting residual inflammatory risk in patients in the chronic phase after AMI (22), the early inflammatory response during AMI has not shown any breakthrough clinical success so far (23, 24). Thus, the task remains to identify ideal targets for acute excessive inflammation outbreaks and effective and safe agents against these targets in AMI. Our study elucidated the role of S100a9 lactylation in acute inflammation as an intrinsic trigger following MI/R, investigated the potential of lactylation as a therapeutic target and biomarker, and established a foundation for the development of pharmacological interventions. The key findings include: (1) Demonstration of neutrophil S100a9 lactylation and its transcriptional regulation; (2) Lactylated S100a9 was released via NETs and triggered cardiomyocyte death by impairing mitochondrial function; (3) Identification of specific lactyltransferase DLAT and its inhibitor ALA; (4) Blockade of

lactylation signaling driven by DLAT improved cardiac function post-MI/R; (6) Independent association of S100a9K26la with cardiac death in AMI patients post-PCI.

Recently, histone lactylation, as a post-transcriptional modification, is found to play diverse roles in different cells during myocardial infarction and other diseases (25-28). In addition, nonhistone protein lactylation, a precise and direct factor, plays a critical role in cardiac fibrosis and heart failure (12, 14). However, the function of lactylation on neutrophils during MI/R remains unexplored. In this study, we demonstrate that neutrophil S100a9 lactylation is elevated early and triggers cardiomyocyte death and neutrophil recruitment post-MI/R. Given that lactylated S100a9 and unlactylated S100a9 had a similar effect on mitochondrial dysfunction and cardiomyocyte death, lactylation did not contribute to the role of secreted S100a9 on cardiomyocyte death. However, S100a9K26R substantially reduced the inflammation and cardiac dysfunction induced by recombinant S100a9, indicating that lactylated S100a9 has a specific disadvantage on MI/R mice that differs from S100a9. Actually, lactylation modified S100a9 and promoted S100a9 translocating into nuclei of neutrophils. There, lactylated S100a9 specifically boosted the expression of *Cxcr1*, *Rhoj*, and *Itga2* post-MI/R, directing cell polarization, adhesion and migration. As sentinels of inflammation, neutrophils are primarily mobilized from BM and recruited to the infarcted heart after MI/R. Then in the heart, neutrophils aggravate the damage through secretion of damage-associated molecular molecules (DAMPs) and increase cardiomyocyte death in a process involving NETs. Our data indicated that S100a9 lactylation plays an important role in the process of neutrophil migration and recruitment during MI/R. Considering the sanctity of BM, where the stem cell niche was protected from the remnants of lytic cell death, especially neutrophils (29), we proposed a hypothetical paradigm about the functional pattern of S100a9 lactylation. Firstly, in response to MI/R, bone marrow and circulating neutrophils upregulate S100a9 lactylation, which served as a co-activator in neutrophil nuclei to manipulate

transcription of migratory-related genes, promoting their migration toward ischemic heart. Subsequently, neutrophils may undergo NETosis and release lactylated S100a9 locally within the ischemic microenvironment where they additionally cause CM death by impairing mitochondrial function.

From a clinical perspective, S100a9 lactylation levels were significantly elevated in neutrophils and plasma in patients with AMI receiving PCI, who had a significantly increased risk of cardiac death and were more likely to experience cardiac death during long-term follow-up. Although the mechanism by which this might occur is unclear, during the follow-up period, the significantly increased frequency of intercurrent HF and the significant negative correlation between S100a9K26la levels and LVEF at baseline or the first month follow-up both suggested cardiac dysfunction is the important functional mechanism of S100a9 lactylation. In addition, S100a9 lactylation levels exhibited significant associations with pro-inflammation cytokine IL-1β as well as the myocardial injury (CK-MB and cTnI) in AMI patients. Moreover, despite S100a9 being widely recognized as secreted alarmins and numerous studies have reported the cardiac benefits of blocking S100a9 (30-34), the transcriptional regulatory role of S100a9 in neutrophil nuclei has not been reported yet. We demonstrate a nuclear function of a lactylated form of S100a9 protein, discriminating from the extracellular mechanism of secreted S100a9. Deletion of neutrophil S100a9K26 lactylation resulted in the suppression of cardiac inflammation and cardiac dysfunction post-MI/R. These findings underscore the direct pathological impact of S100a9 lactylation on MI/R. Collectively, S100a9 lactylation represents a pathological mechanism and probably be a key acute inflammatory target to specifically minimize cardiac neutrophil counts and acute excessive inflammation following MIR and a promising alternative biomarker for evaluating acute inflammatory injury and late prognosis.

Neutrophil counts positively correlate with adverse clinical outcomes in patients with

cardiovascular disease (3). Targeting neutrophil numbers may represent a strategy for treating MI/R (35, 36). Currently, reducing neutrophil burden by inhibiting neutrophil migration and recruitment stands as an important therapeutic approach (37). However, the redundancy of chemokines during neutrophil recruitment poses challenges in transitioning chemokine targeting from preclinical models to clinical trials (38). Therefore, targeting the intrinsic pathway that induces neutrophil migration may represent a therapeutic approach for reducing neutrophil burden (39, 40). Our study revealed that S100a9 lactylation was elevated during neutrophil burst following MI/R and declined as cardiac-infiltrating neutrophils gradually decreased, serving as an intrinsic regulator that enhances neutrophil migration to the injured heart. Although this study did not specifically investigate cardiac-resident neutrophils or bone marrow granulopoiesis, impaired neutrophil migration resulting from lactylation offers a crucial mechanistic basis for the observed reduction in cardiac neutrophil infiltration. These findings highlight the potential application of targeting neutrophil S100a9 lactylation to specifically minimize cardiac neutrophil counts during the neutrophil overload period post-MI/R.

Neutrophils are generally considered detrimental in the setting of acute MI, yet they have been shown to be required for the subsequent cardiac repair processes through anti-inflammation, pro-angiogenesis, and induction of pro-reparative macrophage phenotype (41-43). As reported, 7–14 days after infarction, neutrophil depletion led to worsening of heart function (41). Additionally, short-term S100A9 blockade after injury improves cardiac function, but prolonged inhibition for 7 or 21 days led to progressive deterioration of cardiac function and left ventricular dilation (30, 44). Therefore, the precise timing of targeting neutrophils and their inflammatory mediators is crucial in determining the outcome of myocardial infarction. In our study, pharmacological and genetic inhibition of the DLAT-S100a9K26la pathway during the early stage of MI/R substantially inhibited the neutrophil infiltration and improved cardiac function. However, it is uncertain whether targeting this

pathway more than 7-21 days post-MI/R is detrimental to cardiac healing through disrupting the beneficial roles of neutrophils in anti-inflammation, pro-angiogenesis, and promoting pro-reparative macrophage phenotype. Although S100a9K26R knock-in did not affect immune cells on day 14 post-MI/R, further research is needed to evaluate the long-term consequences of modulating this pathway after MI/R.

Our study elucidates the mechanism underlying the increase in S100a9 lactylation during MI/R, identifying a lactyltransferase DLAT. As an indispensable part of cellular metabolism (45), DLAT catalyzes the conversion of pyruvate to acetyl CoA. We revealed that DLAT functions as a lactyltransferase to catalyze lactylation of S100a9, thereby mediating migration gene expression, highlighting a non-metabolic function of this protein in regulating neutrophil behavior. ALA was confirmed to be able to inhibit lactylation and reduce migration ability of neutrophils, leading to improvement of cardiac function of MI/R mice. Importantly, as a clinical medicine for the treatment of diabetes peripheral neuropathy, clinical trials suggested that lipoic acid was verified that could reduce pain intensity of type 2 diabetes mellitus patients with painful diabetic peripheral neuropathy and improve insulin sensitivity in pre-diabetic subjects (46-48). Moreover, lipoic acid can improve endothelial dysfunction in subjects with impaired fasting glucose or type 2 diabetes (49-51). Based on our work and previous reports, lipoic acid is likely to show a potential application prospect in a precisely targeted anti-inflammatory strategy in patients with AMI, especially AMI patients with diabetes. Thus, ALA might be a promising pharmacological therapy to protect against MI/R and deserves further clinical research to explore its clinical usability.

In summary, our results provide the first evidence of the elevation of S100a9 lactylation in neutrophils in MI/R mice and patients with AMI receiving PCI. DLAT-catalyzed S100a9 lactylation triggers migration-related genes activation in neutrophils in the early stage of MI/R and aggravates the reperfusion injury through amplifying acute inflammation. ALA or

S100a9K26la antibody are promising agent strategies to attenuate cardiac dysfunction post-MI/R through blocking S100a9 lactylation driven by DLAT. Given the marked association with cardiac death in AMI patients, S100a9K26la may be a therapeutic target and clinical prognostic biomarker for MI/R.

This study had several limitations. First, we did not investigate other modifications of S100a9, such as PhosphoS100a9 (52), and the complex crosstalk mechanism of the post-translational modification of S100a9 warrants further investigation. Secondly, the reliability of our clinical conclusions is limited by the single-center and small-sample studies; therefore, further validation through multicenter studies with larger sample sizes is imperative. Additionally, only male mice were used in the mice study, while female subjects were present in the human analyses; therefore, additional validation of this pathway is required in female mice.

Methods

A detailed description of Materials and Methods is provided in the supplemental information.

Sex as a biological variable

Our study exclusively examined male mice. It is unknown whether the findings are relevant for female mice.

Statistical Analysis

Data were reported as mean ± standard deviation (SD) or median (interquartile ranges, 25th-75th percentile). We use Shapiro-Wilk test, Kolmogorov-Smirnov or q-q-plots for

normality and lognormality tests. For comparisons, normally distributed data were analyzed by unpaired 2-tailed Student t test (two-group analysis), and one-way ANOVA or two-way ANOVA with Turkey's test was used to compare multiple data groups affected by one or two independent variables, respectively. Data sets that did not follow a normal distribution were analyzed by Mann-Whitney test (two-group analysis) or Dunn's multiple comparisons test (multiple-group analysis). Tests used to assess significance are detailed in each Figure legend. All statistical analyses were conducted using GraphPad Prism 9.0 software. $P<0.05$ was considered as significant. COX regression model of S100a9K26la levels for events of survival or death, estimated HR, 95% CIs, and p values were calculated. The optimum cutoff of S100a9K26la for discerning MI/R patients and events of survival or death was assessed by receiver-operating curve (ROC) analysis. Kaplan-Meier survival curves (log-rank test) were used for overall survival (OS) analysis using SPSS V.26.0 (IBM Corp, Armonk, NY, USA). The correlation between S100a9K26la levels and other molecules was analysed by Spearman. A linear regression line (red line) with 95% confidence intervals (red area) is shown (P value from the unpaired two-sided t test).

Study approval

All human studies were approved by the Research Ethics Committee of the Second Affiliated Hospital of Harbin Medical University Heilongjiang, China (approval #KY2023-055). All animal experiments in this study were approved by the Research Ethics Committee of the Second Affiliated Hospital of Harbin Medical University Heilongjiang, China (approval #YJSDW2022-167).

Data availability

The supporting data for the findings of this study are available from the corresponding authors upon request. Transcriptome data can be accessed from the Gene Expression Omnibus database under the accession number GSE221740. Mass spectrometry proteomics data from

this study have been deposited in the iProX database under accession number IPX0006753000. The values for all data points in the graphs are reported in the Supporting Data Values file.

Author Contributions.

X.W., X.Y., and G.M. performed study concept and design, review and revision of the paper; X.W., X.Y., Y.C., J.S. and S.L. performed development of methodology, investigation and validation; X.W., X.Y., D.W., P.S., W.S., Z.J., and P.Z. performed investigation and validation; X.W., X.Y., Z.T., P.W., J.Y., C.J., Q.Y. and Y.Z. provided acquisition, analysis and interpretation of data, and statistical analysis; G.M., M.S., M.L., N.W., and T.C. provided technical and material support. M.Z., Y.J., G.M., X.W., and B.Y. performed supervision, project administration. The order of co–first authors was determined by the volume of work each contributed to the study. All authors read and approved the final paper.

Acknowledgement

We are grateful to Dr. Jiaqi Jin for providing help with immunofluorescence staining and Dr. Yubo Yang and Dr. Yang Yang for their assistance with bioinformatics. We thank PTM Bio for the proteomics analysis and OE Biotech for the RNA-seq and CUT-Tag analyses. We would like to thank Editage (www.editage.com) for English language editing.

Funding

This work was supported by the National Natural Science Foundation of China (82270525, 82202272, and 82470521) and the Key Research and Development Program of Heilongjiang Province (GA23C006).

References

1. Hausenloy DJ, and Yellon DM. Ischaemic conditioning and reperfusion injury. *Nat Rev Cardiol.* 2016;13(4):193-209.

2. Yellon DM, and Hausenloy DJ. Myocardial reperfusion injury. *N Engl J Med.* 2007;357(11):1121-35.

3. Luo J, et al. Neutrophil counts and cardiovascular disease. *Eur Heart J.* 2023;44(47):4953-64.

4. Sreejit G, et al. Emerging roles of neutrophil-borne S100A8/A9 in cardiovascular inflammation. *Pharmacol Res.* 2020;161:105212.

5. Zhang Q, and Cao X. Epigenetic Remodeling in Innate Immunity and Inflammation. *Annu Rev Immunol.* 2021;39:279-311.

6. Liu Y, et al. m(6)A demethylase ALKBH5 is required for antibacterial innate defense by intrinsic motivation of neutrophil migration. *Signal Transduct Target Ther.* 2022;7(1):194.

7. Rönnerblad M, et al. Analysis of the DNA methylome and transcriptome in granulopoiesis reveals timed changes and dynamic enhancer methylation. *Blood.* 2014;123(17):e79-89.

8. Pan T, et al. Immune effects of PI3K/Akt/HIF-1α-regulated glycolysis in

polymorphonuclear neutrophils during sepsis. *Crit Care.* 2022;26(1):29.

9. Khatib-Massalha E, et al. Lactate released by inflammatory bone marrow neutrophils induces their mobilization via endothelial GPR81 signaling. *Nat Commun.* 2020;11(1):3547.

10. Chen J, et al. CREB1-driven CXCR4(hi) neutrophils promote skin inflammation in mouse models and human patients. *Nat Commun.* 2023;14(1):5894.

11. Zhang D, et al. Metabolic regulation of gene expression by histone lactylation. *Nature.* 2019;574(7779):575-80.

12. Fan M, et al. Lactate promotes endothelial-to-mesenchymal transition via Snail1 lactylation after myocardial infarction. *Sci Adv.* 2023;9(5):eadc9465.

13. Wang N, et al. Histone Lactylation Boosts Reparative Gene Activation Post-Myocardial Infarction. *Circ Res.* 2022;131(11):893-908.

14. Zhang N, et al. α-myosin heavy chain lactylation maintains sarcomeric structure and function and alleviates the development of heart failure. *Cell Res.* 2023;33(9):679-98.

15. Wang Y, et al. Exercise-induced endothelial Mecp2 lactylation suppresses atherosclerosis via the Ereg/MAPK signalling pathway. *Atherosclerosis.* 2023;375:45-58.

16. Vogl T, et al. Autoinhibitory regulation of S100A8/S100A9 alarmin activity locally restricts sterile inflammation. *J Clin Invest.* 2018;128(5):1852-66.

17. Wang JA-O, et al. Acetate reprogrammes tumour metabolism and promotes PD-L1 expression and immune evasion by upregulating c-Myc. (2522-5812 (Electronic)).

18. Urban CF, et al. Neutrophil extracellular traps contain calprotectin, a cytosolic protein complex involved in host defense against Candida albicans. *PLoS Pathog.*

2009;5(10):e1000639.

19. Shan C, et al. Lysine acetylation activates 6-phosphogluconate dehydrogenase to promote tumor growth. (1097-4164 (Electronic)).

20. Mathias RA, et al. Sirtuin 4 is a lipoamidase regulating pyruvate dehydrogenase complex activity. (1097-4172 (Electronic)).

21. Bielarczyk H, et al. RS-alpha-lipoic acid protects cholinergic cells against sodium nitroprusside and amyloid-beta neurotoxicity through restoration of acetyl-CoA level. (0022-3042 (Print)).

22. Jinagal J, and Dhiman P. Retraction: Retinal Hemorrhage from Blunt Ocular Trauma. N Engl J Med 2019;381:2252. (1533-4406 (Electronic)).

23. Broch K, et al. Randomized Trial of Interleukin-6 Receptor Inhibition in Patients With Acute ST-Segment Elevation Myocardial Infarction. (1558-3597 (Electronic)).

24. Matter MA-O, et al. Inflammation in acute myocardial infarction: the good, the bad and the ugly. (1522-9645 (Electronic)).

25. Gu J, et al. Tumor metabolite lactate promotes tumorigenesis by modulating MOESIN lactylation and enhancing TGF-β signaling in regulatory T cells. *Cell Rep.* 2022;39(12):110986.

26. Jia M, et al. ULK1-mediated metabolic reprogramming regulates Vps34 lipid kinase activity by its lactylation. *Sci Adv.* 2023;9(22):eadg4993.

27. Xiong J, et al. Lactylation-driven METTL3-mediated RNA m(6)A modification promotes immunosuppression of tumor-infiltrating myeloid cells. *Mol Cell.* 2022;82(9):1660-77.e10.

28. Yu J, et al. Histone lactylation drives oncogenesis by facilitating m(6)A reader protein

YTHDF2 expression in ocular melanoma. *Genome Biol.* 2021;22(1):85.

29. Sreejit G, et al. Retention of the NLRP3 Inflammasome-Primed Neutrophils in the Bone Marrow Is Essential for Myocardial Infarction-Induced Granulopoiesis. *Circulation.* 2022;145(1):31-44.

30. Marinković G, et al. Inhibition of pro-inflammatory myeloid cell responses by short-term S100A9 blockade improves cardiac function after myocardial infarction. *Eur Heart J.* 2019;40(32):2713-23.

31. Li Y, et al. S100a8/a9 Signaling Causes Mitochondrial Dysfunction and Cardiomyocyte Death in Response to Ischemic/Reperfusion Injury. *Circulation.* 2019;140(9):751-64.

32. Sreejit G, et al. Neutrophil-Derived S100A8/A9 Amplify Granulopoiesis After Myocardial Infarction. *Circulation.* 2020;141(13):1080-94.

33. Frangogiannis NG. S100A8/A9 as a therapeutic target in myocardial infarction: cellular mechanisms, molecular interactions, and translational challenges. *Eur Heart J.* 2019;40(32):2724-6.

34. Nagareddy PR, et al. NETosis Is Required for S100A8/A9-Induced Granulopoiesis After Myocardial Infarction. *Arterioscler Thromb Vasc Biol.* 2020;40(11):2805-7.

35. Ridker PM, et al. Antiinflammatory Therapy with Canakinumab for Atherosclerotic Disease. *N Engl J Med.* 2017;377(12):1119-31.

36. Ridker PM, et al. Low-Dose Methotrexate for the Prevention of Atherosclerotic Events. *N Engl J Med.* 2019;380(8):752-62.

37. Ocana A, et al. Neutrophils in cancer: prognostic role and therapeutic strategies. *Mol Cancer.* 2017;16(1):137.

38. Schall TJ, and Proudfoot AE. Overcoming hurdles in developing successful drugs targeting chemokine receptors. *Nat Rev Immunol.* 2011;11(5):355-63.

39. Kempf T, et al. GDF-15 is an inhibitor of leukocyte integrin activation required for survival after myocardial infarction in mice. *Nat Med.* 2011;17(5):581-8.

40. Drechsler M, et al. Annexin A1 counteracts chemokine-induced arterial myeloid cell recruitment. *Circ Res.* 2015;116(5):827-35.

41. Horckmans M, et al. Neutrophils orchestrate post-myocardial infarction healing by polarizing macrophages towards a reparative phenotype. *Eur Heart J.* 2017;38(3):187-97.

42. Ferraro B, et al. Pro-Angiogenic Macrophage Phenotype to Promote Myocardial Repair. *J Am Coll Cardiol.* 2019;73(23):2990-3002.

43. Fullerton JN, and Gilroy DW. Resolution of inflammation: a new therapeutic frontier. *Nat Rev Drug Discov.* 2016;15(8):551-67.

44. Marinković G, et al. S100A9 Links Inflammation and Repair in Myocardial Infarction. *Circ Res.* 2020;127(5):664-76.

45. Long DL, et al. Glutathionylation of pyruvate dehydrogenase complex E2 and inflammatory cytokine production during acute inflammation are magnified by mitochondrial oxidative stress. (2213-2317 (Electronic)).

46. Won JA-O, et al. γ-Linolenic Acid versus α-Lipoic Acid for Treating Painful Diabetic Neuropathy in Adults: A 12-Week, Double-Placebo, Randomized, Noninferiority Trial. (2233-6087 (Electronic)).

47. Gosselin LE, et al. Metabolic effects of α-lipoic acid supplementation in pre-diabetics: a randomized, placebo-controlled pilot study. (2042-650X (Electronic)).

48. Ziegler D, et al. Treatment of symptomatic diabetic polyneuropathy with the antioxidant alpha-lipoic acid: a 7-month multicenter randomized controlled trial (ALADIN III Study). ALADIN III Study Group. Alpha-Lipoic Acid in Diabetic Neuropathy. (0149-5992 (Print)).

49. Xiang G, et al. α-lipoic acid can improve endothelial dysfunction in subjects with impaired fasting glucose. (1532-8600 (Electronic)).

50. Heinisch BB, et al. Alpha-lipoic acid improves vascular endothelial function in patients with type 2 diabetes: a placebo-controlled randomized trial. (1365-2362 (Electronic)).

51. Sola S, et al. Irbesartan and lipoic acid improve endothelial function and reduce markers of inflammation in the metabolic syndrome: results of the Irbesartan and Lipoic Acid in Endothelial Dysfunction (ISLAND) study. (1524-4539 (Electronic)).

52. Schenten V, et al. Secretion of the Phosphorylated Form of S100A9 from Neutrophils Is Essential for the Proinflammatory Functions of Extracellular S100A8/A9. *Front Immunol.* 2018;9:447.

Figure legend

Figure 1. Global view of lactylated proteins and identification of S100a9 lactylation in neutrophils under MI/R. (**A–G**) Total and lactylated (Kla) proteomes of BM neutrophils from sham and post-MI/R mice on day 1. (**A**) Number of proteins exhibiting substantial protein level changes in the total proteome after MI/R. (**B**) Number of Kla sites and proteins exhibiting significant Kla changes after MI/R. (**C**) Bubble plot of the top ten GO terms representing the functions of proteins that exhibited upregulated Kla changes. (**D**) Domain analysis of proteins exhibiting upregulated Kla expression. (**E**) Quantitation of Kla S100a8, S100a9, and S100a11 peptides in neutrophils by mass spectrometry. (**F**) Illustration of S100a9 Kla sites identified in neutrophils. (**G**) MS/MS spectrum of the lysine 26 lactylated S100a9 peptide (S100a9K26la) derived from neutrophils. (**H–K**) S100a9K26la immunoblots of BM (**H**) and BL neutrophils (**J**) from sham and post-MI/R mice at 4, 12, 24, and 72 h (n=6). Quantitation of S100a9K26la changes in BM (**I**) and BL (**K**) neutrophils normalized to β-actin. Mean ± SD. Statistical tests for (**I and K**): 1-way ANOVA with Tukey's multiple comparison test (*P* values adjusted for 6 comparisons; $^{***}P < 0.001$, and $^{****}P < 0.0001$ for indicated comparisons). (**L**) Immunofluorescence co-staining for Ly6G (red) with S100a9K26la (green) in infarcted hearts 12, 24, and 72 h post-MI/R (scale bar=20 μm, n=3). (**M**) Blood samples were collected from patients with AMI undergoing PCI (MI/R, n=23) or from patients with UA (Con, n=23) within 24 h. (**N**) Immunoblotting and quantification of S100a9K26la in neutrophils from the control and MI/R groups. (**O**) Measurement of plasma S100a9K26la levels by ELISA. Median (interquartile ranges, 25th-75th percentile). Statistical

tests for (**O**): 2-tailed Mann–Whitney test ($^{****}P < 0.0001$ for indicated comparisons). (**P**) Spearman's correlation analysis of S100a9K26la and cTnI (excluding the cTnI values below the level of 0.2ug/L).

Figure 2. Deletion of S100a9K26-specific lactylation improves cardiac function post-MI/R. (**A**) Strategy for constructing S100a9K26R mutant mice and amino acid alterations at the S100a9 mutation site. (**B**) Nucleotide mutation site in the S100a9K26R mice. (**C**) Hematoxylin and eosin (HE) staining of the heart 3 days after MI/R (scale bar=1 mm, n=6). (**D and E**) Fibrotic area quantification and Masson's trichrome staining 14 days after MI/R (scale bar=1 mm, n=6). Mean ± SD. Statistical tests for (**E**): 1-way ANOVA with Tukey's multiple comparison test (*P* values adjusted for 6 comparisons; $^{**}P < 0.01$, and $^{****}P < 0.0001$ for indicated comparisons). (**F and G**) Representative B-mode, M-mode echocardiograms with measurements on day 14 after MI/R (n=8). Mean ± SD. Statistical tests for (**G**): 2-way ANOVA with Tukey's multiple comparison test (*P* values adjusted for 6 comparisons; $^{*}P < 0.05$, $^{***}P < 0.001$, and $^{****}P < 0.0001$ for indicated comparisons. ns, not significant). (**H**) Schematic representation of the for bone marrow transplantation (BMT) protocol: BM samples from wild-type (WT) and S100a9K26R mice were transplanted into WT recipients and allowed to reconstitute for 6 weeks, after which the mice were subjected to MI/R. Neutrophil-specific S100a9K26R and WT mice were injected with 100 μl rS100a9 (1.5 mg/Kg/BW) 4 h after MI/R and other control mice were injected with the same volume of saline. (**I–K**) HE (scale bar=1 mm, n=6, I), Masson's trichrome staining and fibrotic area quantification of the heart after MI/R (scale bar=1 mm, n=6, J and K). (**L-M**) Representative M-mode echocardiograms with measurements (n=8). Mean ± SD. Statistical tests for (**K and M**): 1-way ANOVA with Tukey's multiple comparison test (*P* values adjusted for 6 comparisons; $^{*}P < 0.05$, $^{**}P < 0.01$, $^{***}P < 0.001$, and $^{****}P < 0.0001$ for indicated

comparisons. ns, not significant).

Figure 3. Lactylated S100a9 is released via NETs and triggers cardiomyocyte death by impairing mitochondrial function. (**A**) ELISA quantification of plasma S100a9K26la levels at various time points post-MI/R (n=9–13). Mean ± SD. Statistical tests for (**A**): 2-way ANOVA with Tukey's multiple comparison test (*P* values adjusted for 6 comparisons; ***$P < 0.001$ and ****$P < 0.0001$ for indicated comparisons). (**B**) Immunofluorescence co-staining of heart tissue for H3Cit (orange), Ly6G (red) with S100a9K26la (green) (scale bar=50 μm, n=5). (**C**) Detection of Plasma S100a9K26la levels from WT and *Padi4*$^{-/-}$ mice 1 day post MI/R by Elisa(n=8). Mean ± SD. Statistical tests for (**C**): unpaired 2-tailed Student t t-test (**$P < 0.01$ for indicated comparisons). (**D**) BM neutrophils were treated with vehicle or PMA (200 nM/L) for 4h. H3Cit (red) with S100a9K26la (green) immunofluorescence co-localization analysis was performed using Zeiss Zen microscope software (scale bar=2μm, n=5). (**E**) BM neutrophils from WT and *Padi4*$^{-/-}$ mice were cultured for 4h with PMA stimulated, cell supernatants were collected for detection of S100a9K26la levels by ELISA (n=8). Mean ± SD. Statistical tests for (**E**): 2-way ANOVA with Tukey's multiple comparison test (*P* values adjusted for 6 comparisons; ****$P < 0.0001$ for indicated comparisons). (**F–J**) NCMs were cultured with NETs from WT and S100a9K26R neutrophils pretreated or untreated with PMA for 24 hours, then collected NCMs to detect ATP levels (**J,** n=5), mitochondrial membrane depolarization (**F and I**, n=5) and Annexin V-APC and PI by flow cytometry (**G and H**, n=5). Mean ± SD. Statistical tests for (**H**–**J**): 2-way ANOVA with Tukey's multiple comparison test (*P* values adjusted for 6 comparisons; ****$P < 0.0001$ for indicated comparisons. ns, not significant).

Figure 4. S100a9K26 lactylation boosts the transcription of neutrophil migration

and promotes neutrophil recruitment post-MI/R. (**A**) Immunoblotting for S100a9K26la, Lamin B1, and GAPDH in cellular fractions of BM neutrophils from WT and S100a9K26R mice day 1 post-MI/R (n=4). (**B and C**) CUT-Tag analysis of S100a9K26la in blood neutrophils from sham and post-MI/R mice on day 1. (**B**) Genes marked by exclusively increased S100a9K26la (S100a9K26la-log2[MI/R/Sham]≥0.5 and S100a9-log2[MI/R/Sham]≤0.5, S100a9K26la-specific), increased in both S100a9K26la and S100a9 (S100a9K26la-log2[MI/R/Sham]>1 and S100a9-log2[MI/R/Sham]>1, shared); or exclusively increased S100a9 (S100a9-log2[MI/R/Sham]≥0.5 and S100a9K26la-log2[MI/R/Sham]≤0.5, S100a9-specific). (**C**) Top 10 GO terms for genes with S100a9K26la-specific modifications. (**D**) The number of upregulated and downregulated genes with and without S100a9K26la binding. (**E**) GO terms of upregulated (red) and downregulated (blue) genes with S100a9K26la modification. (**F**) Representative migration genes ranked by S100a9K26la binding signal (right) and mRNA expression according to the RNA-seq data (left). (**G** and **H**) S100a9K26la occupancy (**G**, n=6) and gene expression (**H**, n=6) in circulating neutrophils at day 1 post-MI/R were analyzed using ChIP-qPCR or RT-qPCR. (**I**) The adhesion of BM neutrophils day 1 post-MI/R in the presence or absence of Mg^{2+} (1 mmol/L) was determined on CMECs pretreated or untreated with TNF-α (20 ng/mL, n=6). (**J**) The percentage of polarized neutrophils (with ruffled or extended pseudopods) day 1 post-MI/R after CXCL2 stimulation. Scale bars, 10 μm (n=5). (**K**) Transwell assay of BM neutrophils day 1 post-MI/R with CXCL2 treated (30 ng/mL) for 2 h (n=4). Median (interquartile ranges, 25th-75th percentile). Statistical tests for (**K**): 2-tailed Mann–Whitney test (*P < 0.05 for indicated comparisons). (**L and M**) Representative flow cytometry plots and quantification of BL (L) and heart (M) neutrophils ($CD45^+CD11b^+Ly6G^+$) from WT and S100a9K26R mice on day 1 post-MI/R (n=5). Mean ± SD. Statistical tests for (**J, L and M**): unpaired 2-tailed Student t t-test. Statistical tests for (**G and H**): 1-way ANOVA with Tukey's multiple comparison test (P values adjusted for 6 comparisons). Statistical tests for (**I**): 2-way

ANOVA with Tukey's multiple comparison test (*P* values adjusted for 6 comparisons). ($^{**}P <$ 0.01, $^{***}P < 0.001$, and $^{***}P < 0.001$ for indicated comparisons. ns, not significant).

Figure 5. DLAT-catalyzed S100a9 lactylation in neutrophils can be antagonized by a-lipoic acid. (**A**) Differentially abundant proteins were identified in neutrophils by IP-MS analysis using anti-S100a9K26la and IgG. (**B**) MS/MS spectrum of DLAT. (**C**) IP assay BM neutrophils post-MI/R with the indicated antibodies (n=4). (**D**) SPR analysis of lactyl-CoA binding to the recombinant DLAT protein. (**E**) An in vitro lactylation assay was performed in the presence or absence of lactyl-CoA (n=4). (**F**) 32Dcl3 cells were differentiated into granulocytes with addition of G-CSF for 4 days and transfected with control small interfering RNA (siRNA; si-NC) or DLAT specific siRNA (si-DLAT) for 24 hours, then collected for immunoblot (n=4). (**G**) Molecular docking between DLAT and lactyl-CoA. (**H**) The per-residue energy contributions of key residues involved in lactyl-CoA combining with DLAT. (**I**) Purified rS100a9 was incubated with immunoprecipitates of Flag-DLAT WT or I423A mutant from HEK293T cells, then detected S100a9K26 lactylation (n=6). (**J and K**) BM neutrophils were stimulated with indicated doses of ALA, then collected for IP assay with anti-DLAT (**J**, n=4) and the intracellular acetyl-CoA detection by ELISA (**K**, n=6). Mean ± SD. Statistical tests for (**K**): 1-way ANOVA with Tukey's multiple comparison test (*P* values adjusted for 6 comparisons; $^{*}P < 0.05$ and $^{**}P < 0.01$ for indicated comparisons. ns, not significant). (**L**) Purified rS100a9 was incubated with immunoprecipitates of Flag-DLAT WT or K131/258R mutant from HEK293T cells, then detected S100a9K26la (n=6). (**M**) An in vitro lactylation assay in the presence or absence of acetyl-CoA (**M**, n=4). (**N and O**) SPR analysis of acetyl-CoA (**N**) or ALA (**O**) binding to the recombinant DLAT protein.(**P and Q**) Flag DLAT plasmid was transfected into HEK293T cells, then collected the cell lysates and incubated with vehicle or lactyl-CoA, acetyl-CoA or ALA, followed by a cellular thermal shift assay

(CETSA, n = 4).

Figure 6. ALA inhibits S100a9 lactylation and improves MI/R. (**A**) Experimental protocol: Mice received intraperitoneal injection of vehicle or ALA (30mg/kg) at different time points. (**B**) S100a9K26la levels in circulating neutrophils were assayed by western blot (n=6). (**C**) Gene expression analysis by RT-qPCR (n=6). (**D**) S100a9K26la occupancy analysis by ChIP-qPCR (n=6). Mean ± SD. Statistical tests for (**B–D**): unpaired 2-tailed Student t t-test ($^{**}P <$ 0.01, $^{***}P < 0.001$, and $^{****}P < 0.0001$ for indicated comparisons. ns, not significant). (**E**) BM neutrophils from vehicle or ALA treated mice at 1 d post-MI/R were collected and treated with CXCL2 (30 ng/mL) for 2 h, and the migration assay was determined by Transwell (n=6). (**F and G**) Representative flow cytometry plots and quantification of cardiac infiltrating $CD45^+CD11b^+Ly6G^-Ly6C^{hi}$ monocytes/macrophages and $CD45^+CD11b^+Ly6G^+$ neutrophils day 1 post-MI/R (n=6). (**H**) Representative images of TUNEL and cTnI double staining and quantitation of TUNEL positive cardiomyocytes (n=6). (**I and K**) Representative M-mode echocardiograms and echocardiogram measurements (n=8). Mean ± SD. Statistical tests for (**E, G, H, J and K**): 2-way ANOVA with Tukey's multiple comparison test (*P* values adjusted for 6 comparisons; $^{****}P < 0.0001$ for indicated comparisons. ns, not significant).

Figure 7. Lactylated S100a9 is associated with cardiac death in AMI patients. (**A**) Flow diagrams of the cardiac death cohort for assessing the plasma S100a9K26la levels and its prognostic value for cardiac death in patients with AMI receiving PCI. The final eligible 94 death cases and 94 survivor-matched controls were enrolled in this cohort according to the occurrence of cardiac death events during 1 year follow-up period. Blood samples were collected from the arterial access site after stent implantation during interventional procedures. **(B)** Plasma levels of S100a9K26la were measured by ELISA. Median (interquartile ranges,

25th-75th percentile). Statistical tests for (**B**): 2-tailed Mann–Whitney test ($^{***}P < 0.001$ for indicated comparisons). (**C**) Spearman's correlation analysis of S100a9K26la and S100a9 with myocardial injury markers and cardiac function indexes. **(D and E)** RNA-seq of circulating $CD45^+$ immune cells from 55 pairs of survivors and deaths, with a volcano plot (**D**) of all genes and Gene Set Enrichment Analysis (**E**) of genes. (**F**) Spearman Correlation Analysis of S100a9K26la and IL-1β. (**G**) Kaplan–Meier plots of long-term cardiac death based on high or low S100a9K26la levels on day 1 post-PCI in patients with AMI.

Figure 1

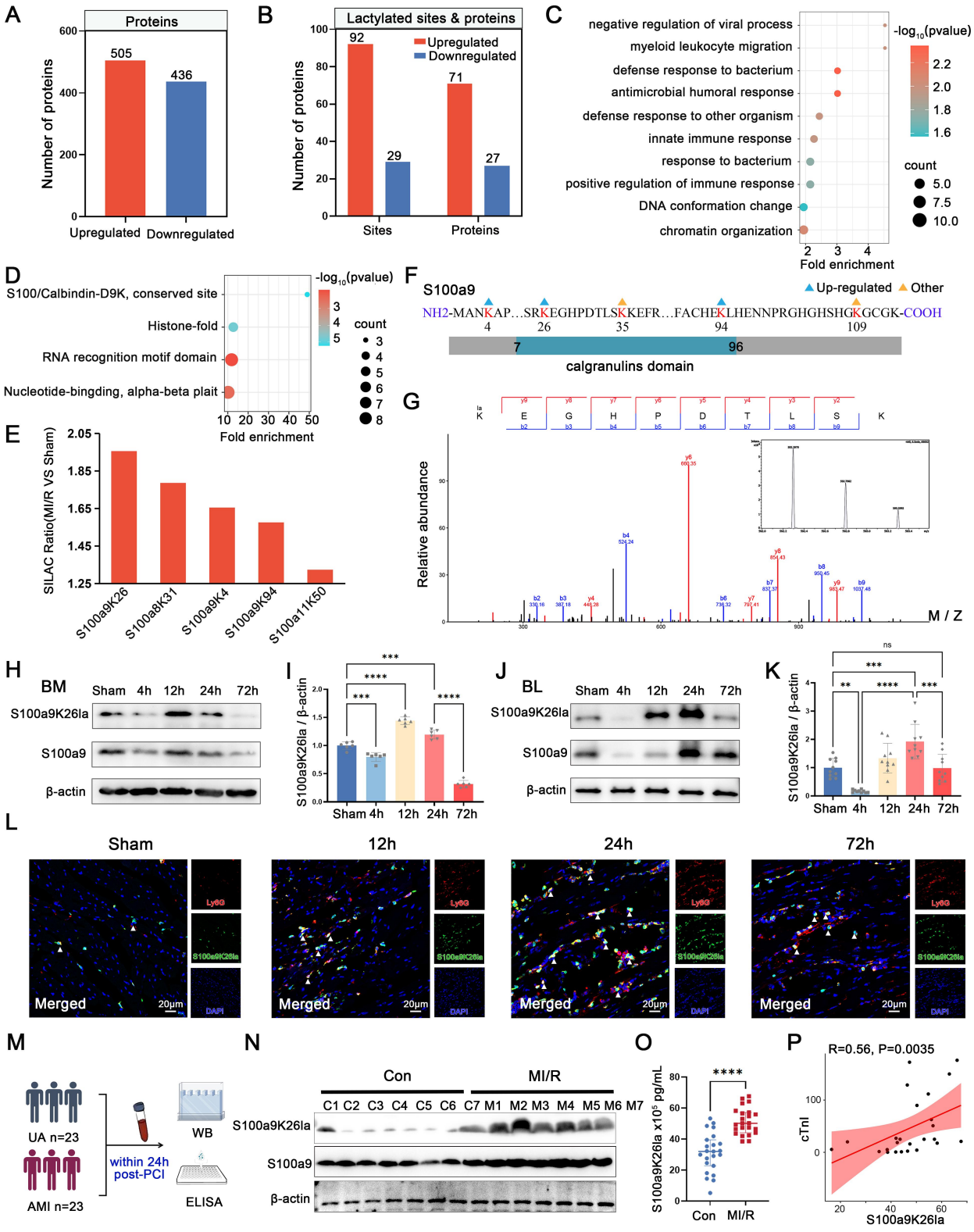
A
Proteins
Number of proteins
505
436
Upregulated
Downregulated
B
Lactylated sites & proteins
Upregulated
Downregulated
92
29
71
27
Sites
Proteins
C
negative regulation of viral process
myeloid leukocyte migration
defense response to bacterium
antimicrobial humoral response
defense response to other organism
innate immune response
response to bacterium
positive regulation of immune response
DNA conformation change
chromatin organization
-log10(pvalue)
count
Fold enrichment
D
S100/Calbindin-D9K, conserved site
Histone-fold
RNA recognition motif domain
Nucleotide-bingding, alpha-beta plait
-log10(pvalue)
count
Fold enrichment
E
SILAC Ratio(MI/R VS Sham)
S100a9K26
S100a8K31
S100a9K4
S100a9K94
S100a11K50
F
S100a9
Up-regulated
Other
NH2-MANKAP…SRKEGHPDTLSKKEFR…FACHEKLHENNPRGHGHSHGKGCGK-COOH
calgranulins domain
G
Relative abundance
M / Z
H
BM
Sham 4h 12h 24h 72h
S100a9K26la
S100a9
β-actin
I
S100a9K26la / β-actin
Sham 4h 12h 24h 72h
J
BL
Sham 4h 12h 24h 72h
S100a9K26la
S100a9
β-actin
K
S100a9K26la / β-actin
Sham 4h 12h 24h 72h
L
Sham
12h
24h
72h
Merged
20μm
M
UA n=23
AMI n=23
within 24h post-PCI
WB
ELISA
N
Con
MI/R
C1 C2 C3 C4 C5 C6 C7 M1 M2 M3 M4 M5 M6 M7
S100a9K26la
S100a9
β-actin
O
S100a9K26la x10^5 pg/mL
Con
MI/R
P
R=0.56, P=0.0035
cTnI
S100a9K26la

Figure 2

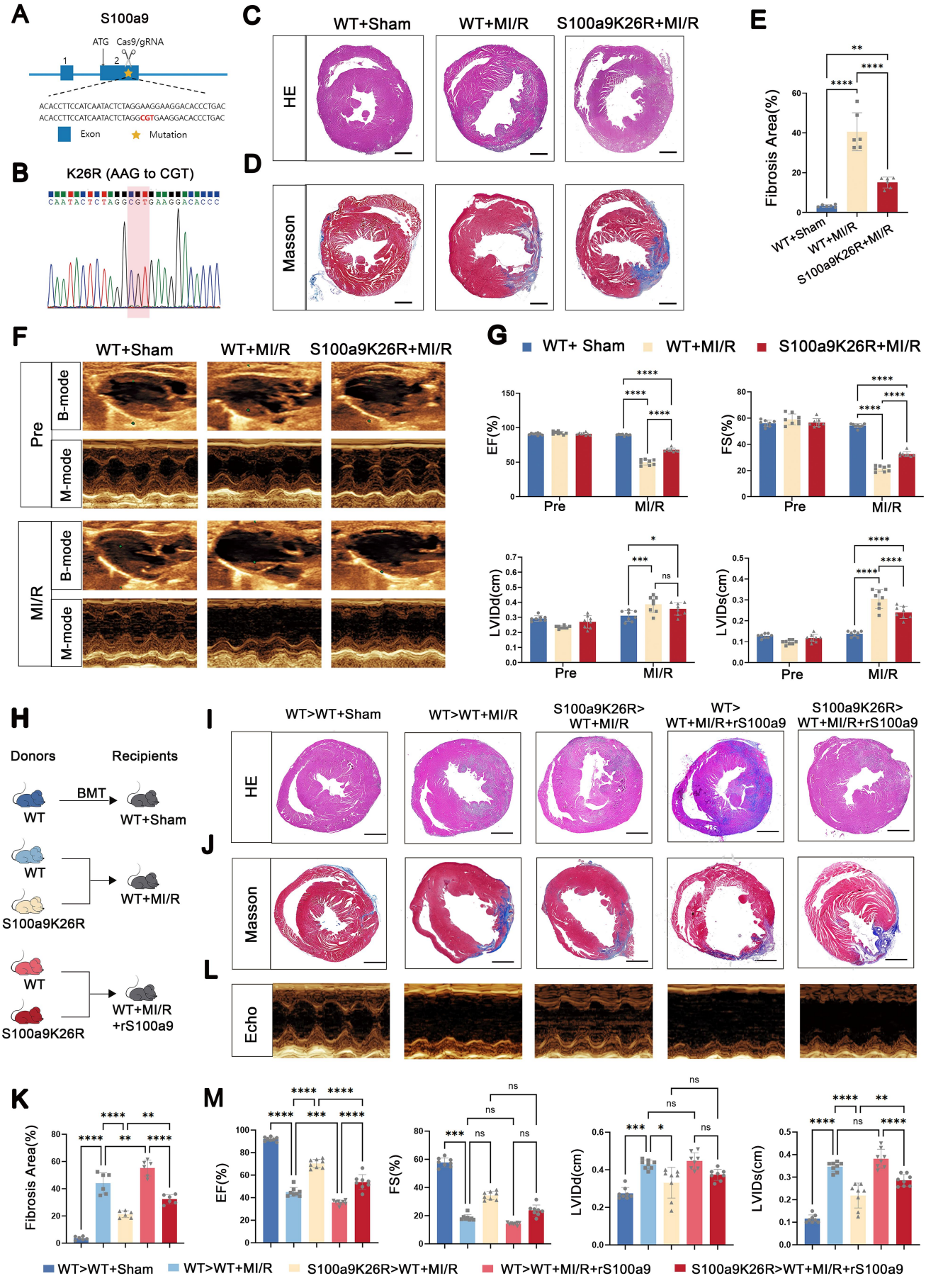
A
S100a9
ATG Cas9/gRNA
ACACCTTCCATCAATACTCTAGGAAGGAAGGACACCCTGAC
ACACCTTCCATCAATACTCTAGGCGTGAAGGACACCCTGAC
Exon
Mutation
B
K26R (AAG to CGT)
C
WT+Sham
WT+MI/R
S100a9K26R+MI/R
HE
D
Masson
E
Fibrosis Area(%)
F
Pre
MI/R
B-mode
M-mode
G
WT+ Sham
WT+MI/R
S100a9K26R+MI/R
EF(%)
FS(%)
LVIDd(cm)
LVIDs(cm)
H
Donors
Recipients
BMT
WT
WT+Sham
S100a9K26R
WT+MI/R
WT+MI/R
+rS100a9
I
WT>WT+Sham
WT>WT+MI/R
S100a9K26R>
WT+MI/R
WT>
WT+MI/R+rS100a9
S100a9K26R>
WT+MI/R+rS100a9
J
Masson
L
Echo
K
Fibrosis Area(%)
M
EF(%)
FS(%)
LVIDd(cm)
LVIDs(cm)
WT>WT+Sham
WT>WT+MI/R
S100a9K26R>WT+MI/R
WT>WT+MI/R+rS100a9
S100a9K26R>WT+MI/R+rS100a9

Figure 3

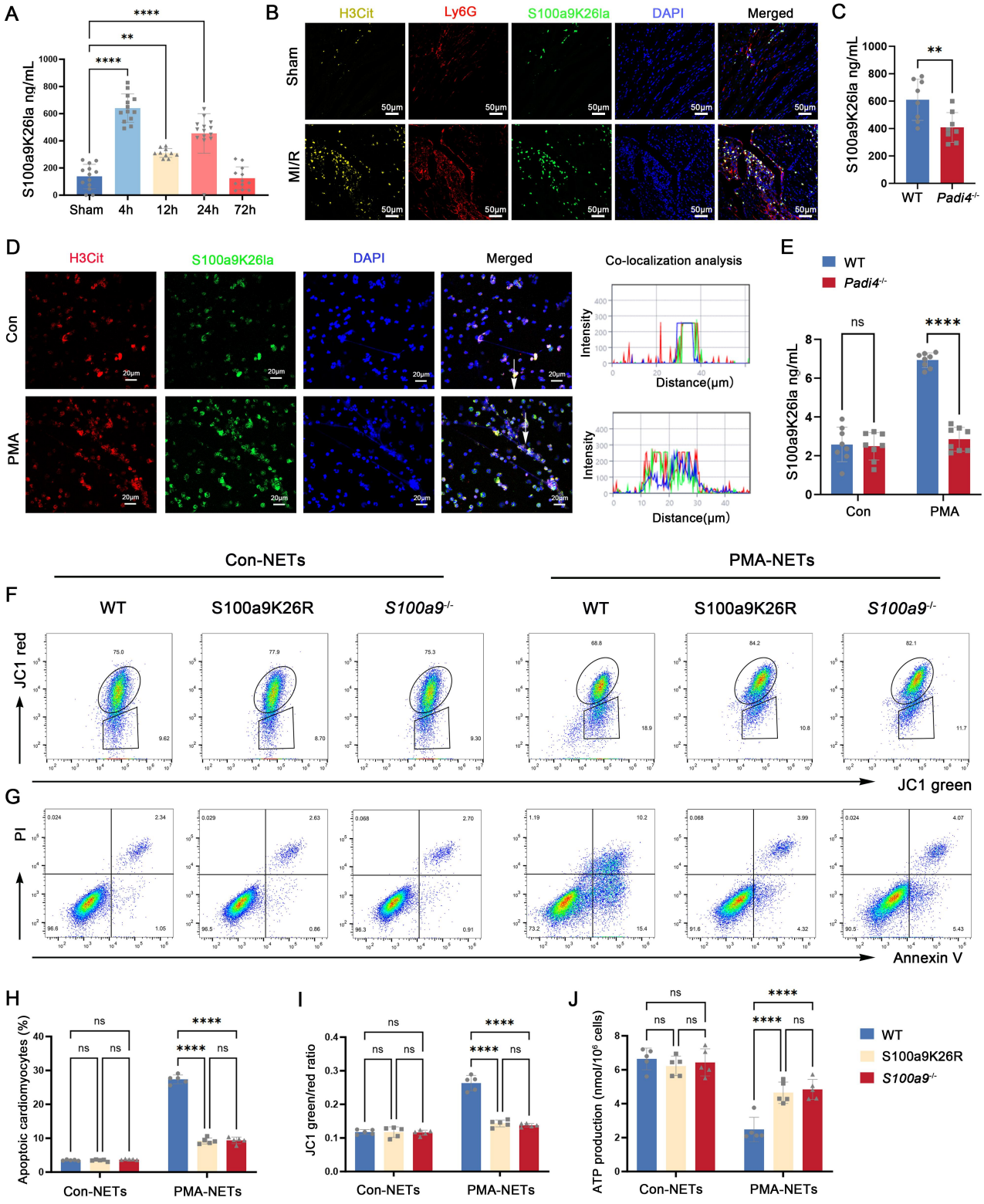
A
S100a9K26la ng/mL
Sham
4h
12h
24h
72h
B
H3Cit
Ly6G
S100a9K26la
DAPI
Merged
Sham
MI/R
C
S100a9K26la ng/mL
WT
Padi4-/-
D
H3Cit
S100a9K26la
DAPI
Merged
Co-localization analysis
Con
PMA
Intensity
Distance(μm)
E
WT
Padi4-/-
S100a9K26la ng/mL
Con
PMA
Con-NETs
PMA-NETs
F
WT
S100a9K26R
S100a9-/-
JC1 red
JC1 green
G
PI
Annexin V
H
Apoptoic cardiomyocytes (%)
Con-NETs
PMA-NETs
I
JC1 green/red ratio
J
ATP production (nmol/10^6 cells)
WT
S100a9K26R
S100a9-/-

Figure 4

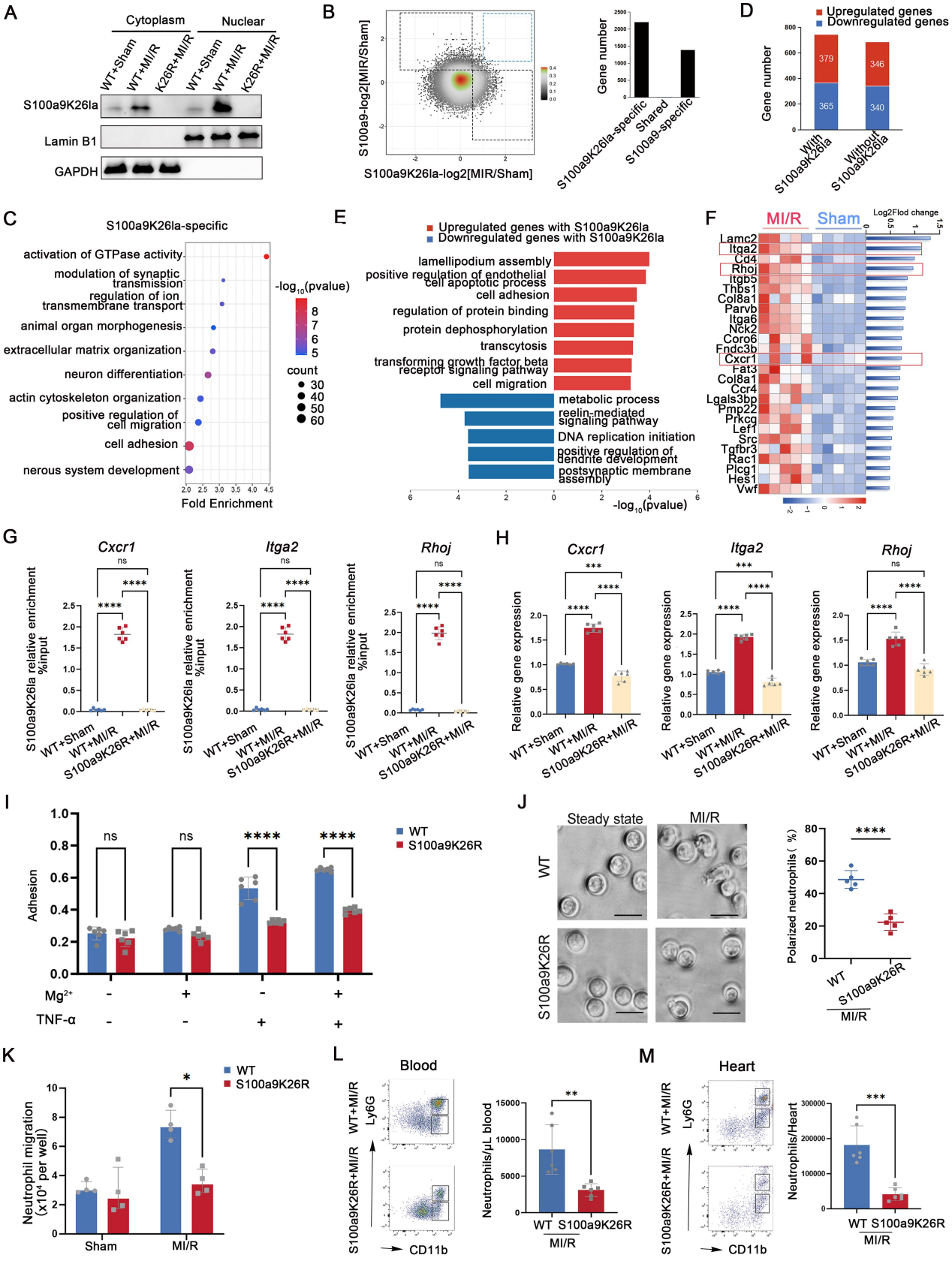
A
Cytoplasm
Nuclear
WT+Sham
WT+MI/R
K26R+MI/R
S100a9K26la
Lamin B1
GAPDH
B
S100a9-log2[MIR/Sham]
S100a9K26la-log2[MIR/Sham]
Gene number
S100a9K26la-specific
Shared
S100a9-specific
D
Upregulated genes
Downregulated genes
Gene number
379
365
346
340
With S100a9K26la
Without S100a9K26la
C
S100a9K26la-specific
activation of GTPase activity
modulation of synaptic transmission
regulation of ion transmembrane transport
animal organ morphogenesis
extracellular matrix organization
neuron differentiation
actin cytoskeleton organization
positive regulation of cell migration
cell adhesion
nerous system development
-log10(pvalue)
count
Fold Enrichment
E
Upregulated genes with S100a9K26la
Downregulated genes with S100a9K26la
lamellipodium assembly
positive regulation of endothelial cell apoptotic process
cell adhesion
regulation of protein binding
protein dephosphorylation
transcytosis
transforming growth factor beta receptor signaling pathway
cell migration
metabolic process
reelin-mediated signaling pathway
DNA replication initiation
positive regulation of dendrite development
postsynaptic membrane assembly
-log10(pvalue)
F
MI/R
Sham
Log2Flod change
Lamc2
Itga2
Cd4
Rhoj
Itgb5
Thbs1
Col8a1
Parvb
Itga6
Nck2
Coro6
Fndc3b
Cxcr1
Fat3
Col8a1
Ccr4
Lgals3bp
Pmp22
Prkcg
Lef1
Src
Tgfbr3
Rac1
Plcg1
Hes1
Vwf
G
Cxcr1
Itga2
Rhoj
S100a9K26la relative enrichment %input
WT+Sham
WT+MI/R
S100a9K26R+MI/R
H
Cxcr1
Itga2
Rhoj
Relative gene expression
I
Adhesion
WT
S100a9K26R
Mg2+
TNF-α
J
Steady state
MI/R
WT
S100a9K26R
Polarized neutrophils (%)
K
Neutrophil migration (x10⁴ per well)
Sham
MI/R
L
Blood
WT+MI/R
S100a9K26R+MI/R
Ly6G
CD11b
Neutrophils/μL blood
M
Heart
Neutrophils/Heart

Figure 5

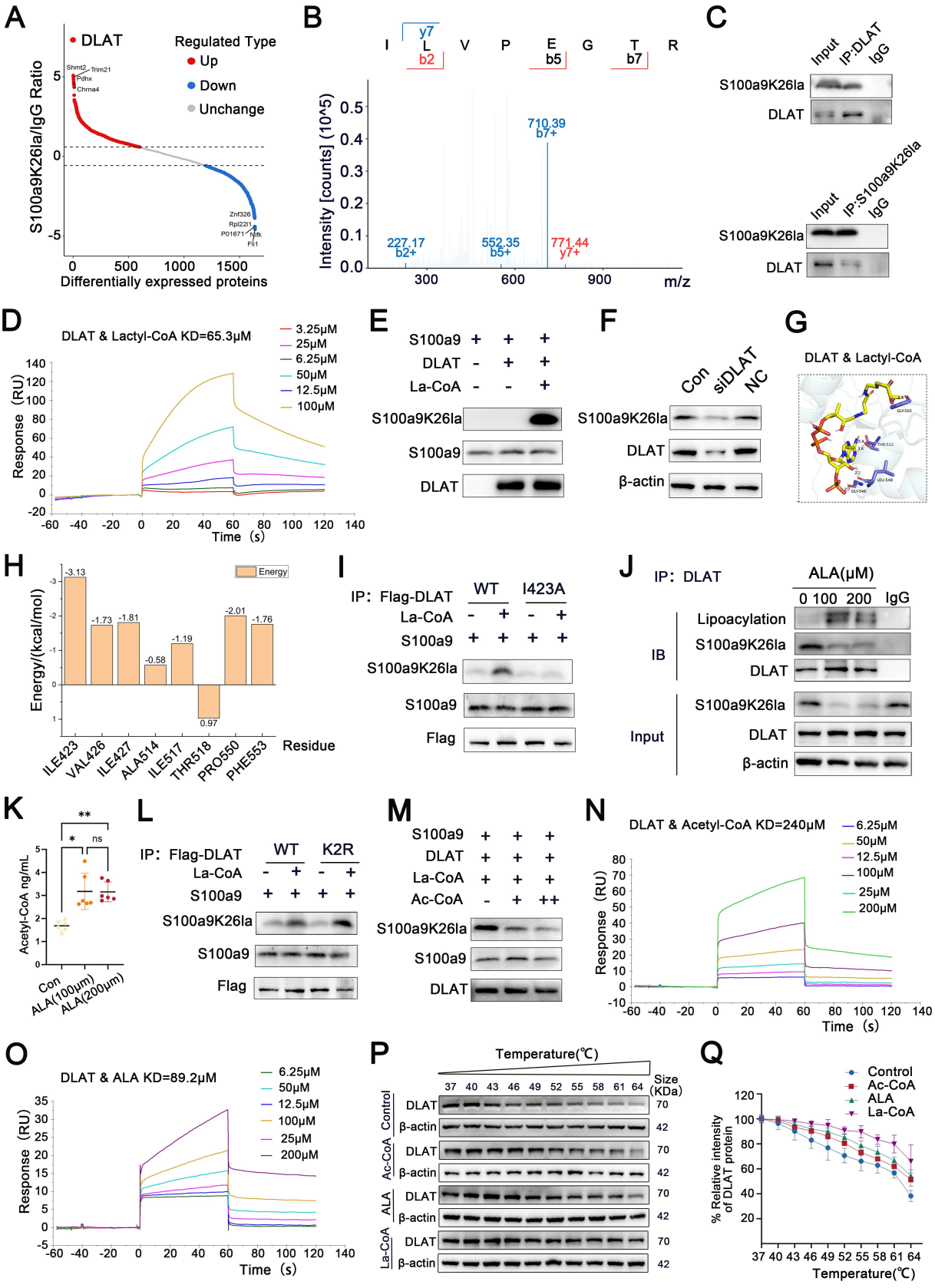
A
DLAT
Regulated Type
Up
Down
Unchange
S100a9K26la/IgG Ratio
Differentially expressed proteins
B
Intensity [counts] (10^5)
m/z
710.39 b7+
227.17 b2+
552.35 b5+
771.44 y7+
C
Input
IP:DLAT
IgG
S100a9K26la
DLAT
IP:S100a9K26la
D
DLAT & Lactyl-CoA KD=65.3μM
3.25μM
25μM
6.25μM
50μM
12.5μM
100μM
Response (RU)
Time (s)
E
S100a9
DLAT
La-CoA
S100a9K26la
S100a9
DLAT
F
Con
siDLAT
NC
S100a9K26la
DLAT
β-actin
G
DLAT & Lactyl-CoA
H
Energy
Energy/(kcal/mol)
-3.13
-1.73
-1.81
-0.58
-1.19
0.97
-2.01
-1.76
ILE423
VAL426
ILE427
ALA514
ILE517
THR518
PRO550
PHE553
Residue
I
IP: Flag-DLAT
WT
I423A
La-CoA
S100a9
S100a9K26la
S100a9
Flag
J
IP: DLAT
ALA(μM)
0 100 200 IgG
IB
Lipoacylation
S100a9K26la
DLAT
Input
S100a9K26la
DLAT
β-actin
K
Acetyl-CoA ng/mL
Con
ALA(100μm)
ALA(200μm)
L
IP: Flag-DLAT
WT
K2R
La-CoA
S100a9
S100a9K26la
S100a9
Flag
M
S100a9
DLAT
La-CoA
Ac-CoA
S100a9K26la
S100a9
DLAT
N
DLAT & Acetyl-CoA KD=240μM
6.25μM
50μM
12.5μM
100μM
25μM
200μM
Response (RU)
Time (s)
O
DLAT & ALA KD=89.2μM
6.25μM
50μM
12.5μM
100μM
25μM
200μM
Response (RU)
Time (s)
P
Temperature(℃)
Size (KDa)
Control
Ac-CoA
ALA
La-CoA
DLAT
β-actin
Q
Control
Ac-CoA
ALA
La-CoA
% Relative intensity of DLAT protein
Temperature(℃)

Figure 6

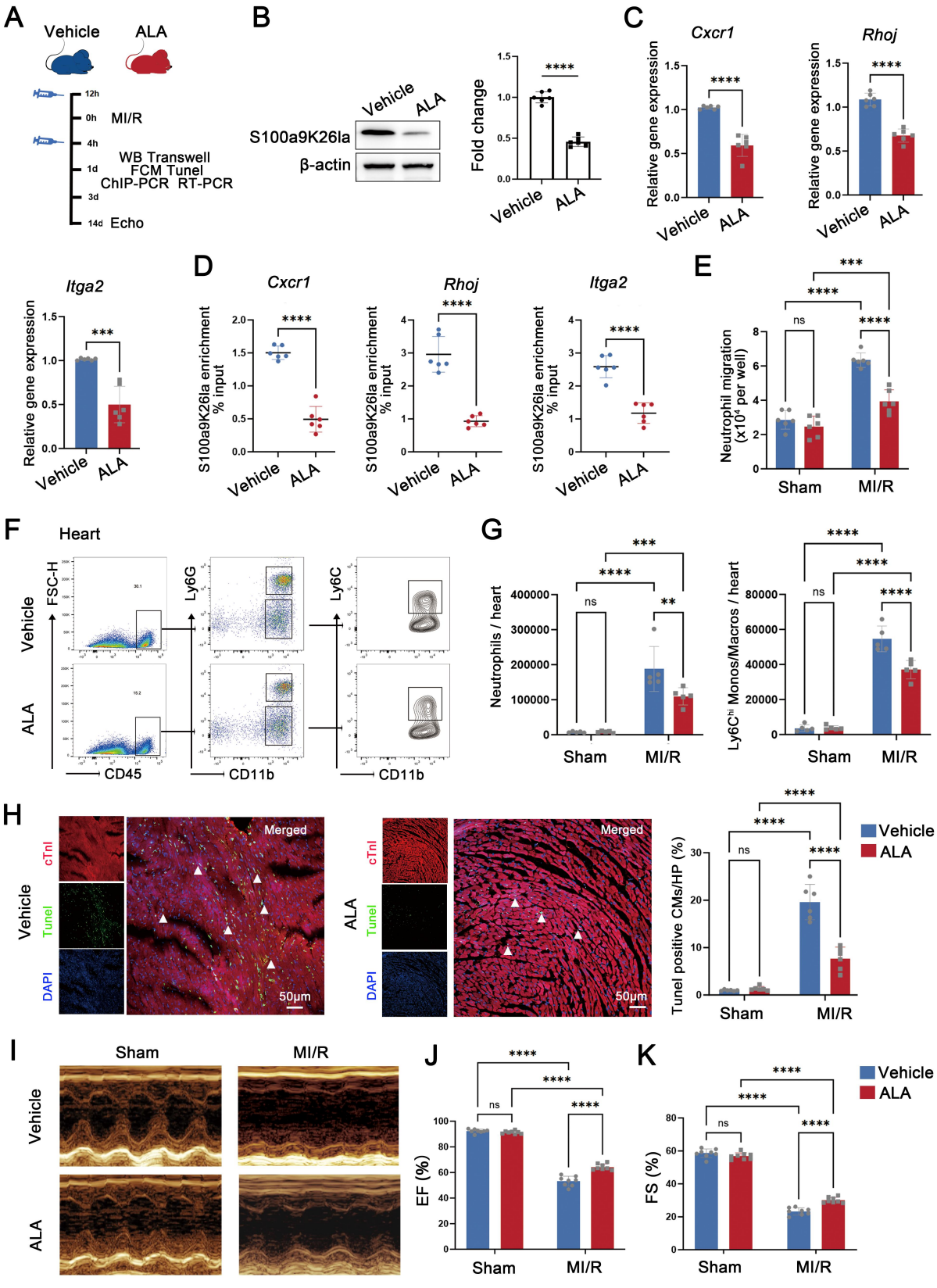
A
Vehicle
ALA
12h
0h MI/R
4h
1d WB Transwell FCM Tunel ChIP-PCR RT-PCR
3d
14d Echo
B
Vehicle
ALA
S100a9K26la
β-actin
Fold change
****
C
Cxcr1
Rhoj
Relative gene expression
****
Itga2
***
D
Cxcr1
Rhoj
Itga2
S100a9K26la enrichment % input
****
E
Neutrophil migration (x10⁴ per well)
***
****
ns
Sham
MI/R
F
Heart
Vehicle
ALA
FSC-H
Ly6G
Ly6C
CD45
CD11b
CD11b
G
Neutrophils / heart
Ly6C^hi Monos/Macros / heart
ns
**
****
***
Sham
MI/R
H
Vehicle
ALA
cTnI
Tunel
DAPI
Merged
50μm
Tunel positive CMs/HP (%)
Vehicle
ALA
I
Sham
MI/R
Vehicle
ALA
J
EF (%)
K
FS (%)

Figure 7

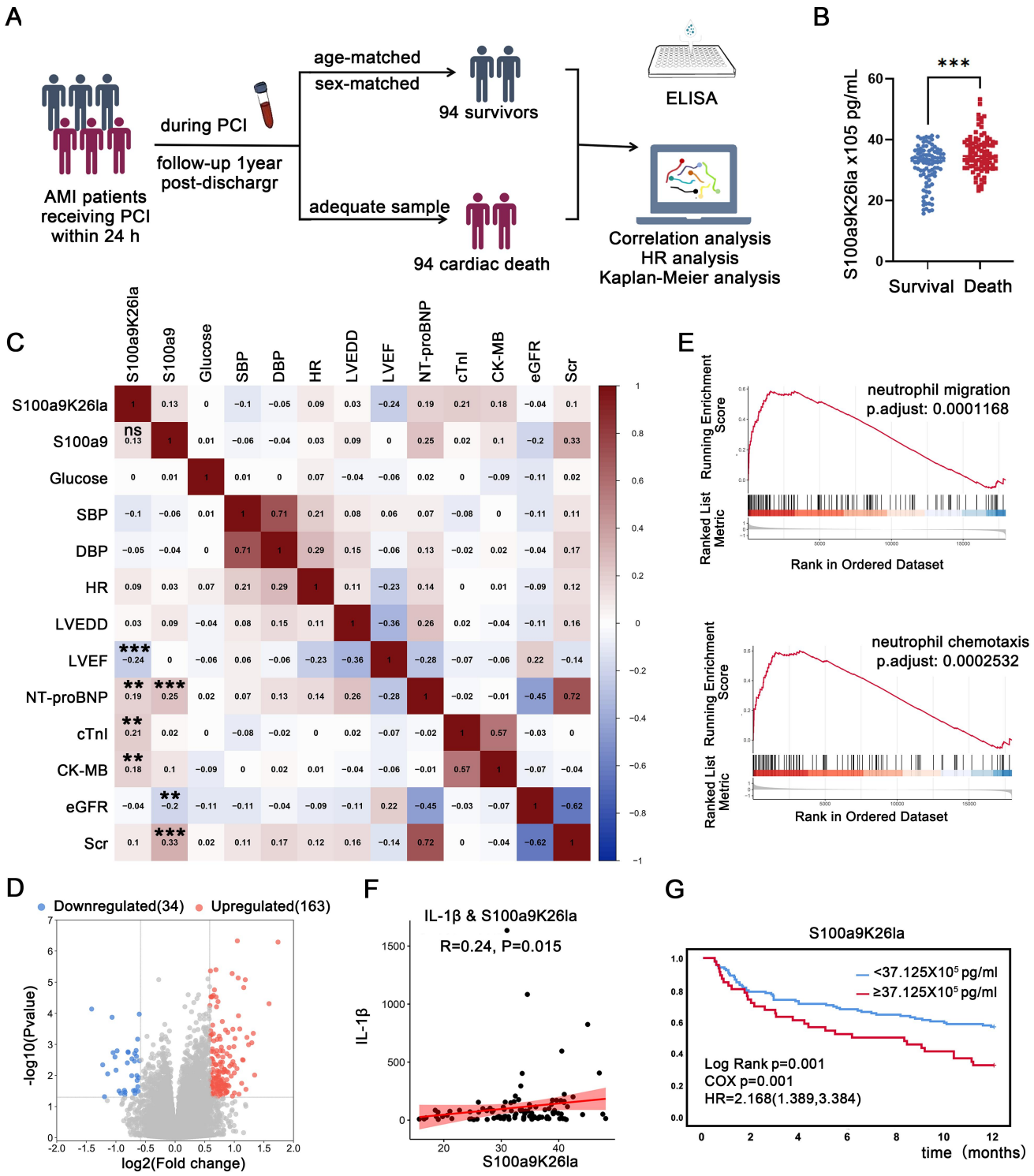
A
AMI patients receiving PCI within 24 h
during PCI
follow-up 1year post-dischargr
age-matched
sex-matched
94 survivors
adequate sample
94 cardiac death
ELISA
Correlation analysis
HR analysis
Kaplan-Meier analysis
B
S100a9K26la x105 pg/mL
***
Survival
Death
C
S100a9K26la
S100a9
Glucose
SBP
DBP
HR
LVEDD
LVEF
NT-proBNP
cTnI
CK-MB
eGFR
Scr
D
Downregulated(34)
Upregulated(163)
-log10(Pvalue)
log2(Fold change)
E
neutrophil migration
p.adjust: 0.0001168
Running Enrichment Score
Ranked List Metric
Rank in Ordered Dataset
neutrophil chemotaxis
p.adjust: 0.0002532
F
IL-1β & S100a9K26la
R=0.24, P=0.015
IL-1β
S100a9K26la
G
S100a9K26la
<37.125X10⁵ pg/ml
≥37.125X10⁵ pg/ml
Log Rank p=0.001
COX p=0.001
HR=2.168(1.389,3.384)
time (months)